

# Efficient Densest Flow Queries in Transaction Flow Networks (Complete Version)

Jixin Jiang<sup>✉</sup>, Yunxiang Zhao<sup>✉</sup>, Lyu Xu<sup>✉</sup>, Byron Choi<sup>✉</sup>, *Fellow, HKIE*  
 Bingsheng He<sup>✉</sup>, *Fellow, IEEE*, Shixuan Sun<sup>✉</sup>, Jia Chen<sup>✉</sup>

**Abstract**—Transaction flow networks are crucial in detecting illicit activities such as wash trading, credit card fraud, cashback arbitrage fraud, and money laundering. Our collaborator, Grab, a leader in digital payments in Southeast Asia, faces increasingly sophisticated fraud patterns in its transaction flow networks. In industry settings such as Grabs fraud detection pipeline, identifying fraudulent activities heavily relies on detecting dense flows within transaction networks. Motivated by this practical foundation, we propose the *S-T densest flow* (STDF) query. Given a transaction flow network  $G$ , a source set  $S$ , a sink set  $T$ , and a size threshold  $k$ , the query outputs subsets  $S' \subseteq S$  and  $T' \subseteq T$  such that the maximum flow from  $S'$  to  $T'$  is densest, with  $|S' \cup T'| \geq k$ . Recognizing the NP-hardness of the STDF query, we develop an efficient divide-and-conquer algorithm, Conan. Driven by industry needs for scalable and efficient solutions, we introduce an approximate flow-peeling algorithm to optimize the performance of Conan, enhancing its efficiency in processing large transaction networks. Our approach has been integrated into Grab’s fraud detection scenario, resulting in significant improvements in identifying fraudulent activities. Experiments show that Conan outperforms baseline methods by up to three orders of magnitude in runtime and more effectively identifies the densest flows. We showcase Conan’s applications in fraud detection on transaction flow networks from our industry partner, Grab, and on non-fungible tokens (NFTs).

**Index Terms**—Graph Anomaly Detection, Densest Flow Query

## I. INTRODUCTION

TRANSACTION flow networks, such as Bitcoin networks [67] and Ethereum networks [64], [46], have become increasingly prevalent in various applications, including e-payment systems [6] and cryptocurrency exchanges [40]. These networks are vulnerable to exploitation by fraudsters for illicit activities, including wash trading [15], credit card fraud [16], and money laundering [62], [31], [48], [14]. In industry, detecting such fraudulent activities is a critical and challenging task due to the scale and complexity of transaction networks. Our industry partner, Grab, has encountered sophisticated fraud patterns that traditional methods fail to detect efficiently. Beyond the Grab setting, dense and temporally constrained fund-flow patterns also serve as a core analytic

Jixin Jiang and Bingsheng He are with National University of Singapore, Singapore. E-mail: {jiangjx,hebs}@comp.nus.edu.sg

Yunxiang Zhao and Byron Choi are with Hong Kong Baptist University, Hong Kong. E-mail: {csyxzhao, bchoi}@comp.hkbu.edu.hk

Lyu Xu is with Nanyang Technological University, Singapore. Email: lyu.xu@ntu.edu.sg.

Shixuan Sun is with Shanghai Jiao Tong University, Shanghai, China. E-mail: sunshixuan@sjtu.edu.cn

Jia Chen is with Grab Holdings, Singapore. Email: jia.chen@grab.com  
 Corresponding author: Yunxiang Zhao.

primitive in antimoney-laundering (AML) systems [52], [68], NFT wash-trading detection [56], [60], credit-card mule-ring identification [47], [43], and cross-border layering analysis [33]. Unlike machine-learning classifiers [17], [19] that operate on individual nodes, these applications require reasoning about global multi-source–multi-sink flow concentration patterns, which motivates a principled graph-analytic formulation. To address the industry challenges, we propose a novel densest flow query that is designed to enhance fraud detection capabilities in practical applications. We first demonstrate the query with the example of money laundering detection.

**Query for Money Laundering.** Money laundering, a financial crime, unfolds in three phases: placement, layering, and integration [61], [57], [42], [43]. It commences with *source accounts* receiving illicit funds, which are subsequently transferred to *sink accounts* (*a.k.a.* destination accounts) to obscure their illegal origins. A critical element in the layering phase is the extensive use of money mules—individuals often in financially vulnerable situations—who conduct numerous transactions to help conceal the funds’ transfer [61]. Despite existing methods like [69] that monitor short-term, high-volume flows between specific source and sink pairs, significant gaps remain when compared to real-world industry scenarios. In industry, dense flow analysis has become a widely used approach for identifying fraudulent patterns, focusing on the concentration of transaction flow within a group rather than individual source-sink pairs. This approach shifts the focus from isolated transactions to detecting suspicious activity among interconnected accounts, enabling the identification and differentiation of fraudsters within groups of suspect accounts. These intermediaries, while moving large sums of money, create an intricate network of transactions that significantly obscures the trail of the original illicit funds. Fraudulent activities often involve substantial transfers within a few accounts, resulting in a pattern of dense financial flows [43]. We refine the concept of density as detailed in [37], [30], [54] to define flow density. In particular, the density of flow from a set of sources to a set of sinks is determined by dividing the flow value by the number of sources and sinks. The occurrence of dense flow among specific sources and sinks is not limited to money laundering; it is also prevalent in other fraudulent activities, such as wash trading and credit card fraud, within transaction flow networks [51], [23]. Such dense multi-hop fund movements cannot be captured by node-level or edge-level ML/GNN classifiers, which do not model the temporally ordered, multi-source–multi-sink propagation

of value. Detecting the densest temporally valid flow therefore constitutes a structural, flow-topological problem rather than a predictive ML task, and motivates the formulation of the STDF query.

**Fraud Detection Pipelines in Grab.** Detecting fraudulent actors in transaction flow networks is a critical challenge for both academia and industry. Densest flow queries have become essential tools for identifying and isolating fraudulent activity patterns [43], [59], [23], [25]. Grab’s fraud detection pipeline, illustrated in Figure 1, consists of the following steps: (a) *Network Construction* the transaction flow network  $G$  where vertices represent users, merchants, or cards, and edges represent transactions with capacities reflecting transaction amounts. Risk control specialists identify sets of accounts exhibiting suspicious behavior, such as abnormal transaction patterns or significant outgoing or incoming flows (labeled as  $S$  and  $T$ , respectively); (b) *Temporal Dependency* analysis of temporal dependencies to capture evolving fraud patterns; (c) *Densest Flow Detection* identification of dense flow patterns indicative of fraudulent behavior using densest flow queries; and (d) *Applications and Operational Requirements* various fraud detection applications such as credit card fraud, wash trading, and cashback arbitrage fraud, along with operational needs like scalability and response time. Similar pipelines are employed by other organizations [43], [70], [37].

Motivated by this fraud detection pipeline, we propose the  $S$ - $T$  densest flow (STDF) query, specifically designed to enhance fraud detection in transaction flow networks. This query addresses the unique challenges posed by such networks. Given disjoint sets  $S$  and  $T$  representing sources and sinks, STDF seeks subsets  $S' \subseteq S$  and  $T' \subseteq T$  that maximize flow density while ensuring that the combined size of these subsets meets or exceeds a minimum threshold  $k$  (i.e.,  $|S'|+|T'| \geq k$ ). This criterion is crucial, as it provides flexibility to detect both key players and peripheral members of fraud organizations, enhancing robustness against evasion tactics like creating excess accounts to dilute flows. Different applications vary in scale: for example, wash trading typically involves smaller groups, credit card fraud operations are medium-sized, and cashback arbitrage fraud schemes often involve a large number of accounts. By adjusting the minimum size threshold  $k$ , STDF can detect fraudulent groups across these varying scales.

**Challenges.** Addressing STDF queries presents two major challenges. *First*, these queries are NP-hard (Section II). A naïve approach would require enumerating all possible combinations of group sizes for  $S$  and  $T$  to find the optimal subsets of  $S$  and  $T$ , involving numerous maximum flow computations. However, maximum flow algorithms themselves have high computational complexities. On large-scale graphs like the Ethereum transaction network, which processed 11.7 million transactions per month in 2021 [64], frequently invoking such computationally intensive algorithms is impractical. *Second*, transaction flow networks, especially those involving fraudulent activities, exhibit unique temporal dependencies. Fraudulent flows often occur in specific temporal patterns. Traditional maximum flow algorithms cannot capture these temporal

dependencies. Therefore, computing maximum flows requires novel algorithms that account for temporal constraints, adding another layer of complexity to the problem.

This paper presents several key contributions to the field of fraud detection in transaction networks, including:

- 1) **Novel Query Formulation:** We introduce the STDF query, motivated by real-world fraud detection scenarios [43], [59], [70] and the needs of our industry partner to identify dense flows in transaction networks.
- 2) **Divide-and-Conquer Algorithm:** We develop a divide-and-CONquer Algorithm for densest flow queries (Conan), that efficiently enumerates subsets of  $S$  and  $T$  to solve densest flow queries.
- 3) **Peeling Algorithm with Theoretical Guarantee:** We propose a peeling algorithm with a 3-approximation theoretical guarantee, significantly reducing the number of maximum flow computations to  $(|S|+|T|)^2$  instances.
- 4) **Pruning Techniques:** We introduce pruning methods to optimize the performance of the 3-approximation algorithm, further enhancing computational efficiency.
- 5) **Industrial Deployment and Impact:** Our methods have been deployed in Grab’s detection pipeline, leading to the discovery of significant fraudulent activities, including credit card fraud and cashback arbitrage fraud. Moreover, Conan has shown substantial impact in public applications; for example, it detects fraudulent behaviors such as wash trading and money laundering in NFT networks.

## II. BACKGROUND

### A. Preliminaries

A **flow network**  $G = (V, E, C)$  is a directed graph, where (a)  $V$  is a set of vertices, with each vertex  $v \in V$  representing an account; (b)  $E \subseteq V \times V$  is a set of edges, with  $(u, v) \in E$  representing a transaction<sup>1</sup>; and (c)  $C$  is a non-negative capacity mapping function, such that  $C(u, v)$  is the capacity on edge  $(u, v) \in E$ , which is the transaction volume. For simplicity, self-loops in the flow network are not considered.

**Definition II.1** (Flow). *Given a flow network  $G = (V, E, C)$  with a source  $s \in V$  and a sink  $t \in V$ , a flow from  $s$  to  $t$  is a mapping function  $f : V \times V \rightarrow \mathbb{R}^+$  satisfying the following:*

- 1) **Capacity Constraint:**  $\forall (u, v) \in E$ , the flow  $f(u, v)$  does not exceed  $C(u, v)$ , i.e.,  $f(u, v) \leq C(u, v)$ .
- 2) **Flow Conservation:**  $\forall u \in V \setminus \{s, t\}$ , the flow into  $u$  equals the flow out of  $u$ , i.e.,  $\sum_{v \in V} f(v, u) = \sum_{v \in V} f(u, v)$ .

The *value* of a flow  $f$  from  $s$  to  $t$  is denoted by  $|f| = \sum_{v \in V} f(s, v)$ . Given a flow network  $G$ , a source  $s$  and a sink  $t$ , the maximum flow problem aims to find a flow  $f$  such that  $|f|$  is maximized and the value is denoted by  $\text{MFLOW}(s, t)$ . The maximum flow problem can be expanded to accommodate multiple sources,  $S$ , and multiple sinks,  $T$ , with

<sup>1</sup>In the case where multiple edges exist between two vertices, exemplified by  $\{e_1, \dots, e_i\}$  between vertices  $u$  and  $v$ , various strategies can be adopted to simplify the graph. One approach is the introduction of an intermediate node for each transaction, effectively transforming graphs with multiple edges into simplified versions without them. Thus, we assume the graphs considered in this study do not contain multiple edges.

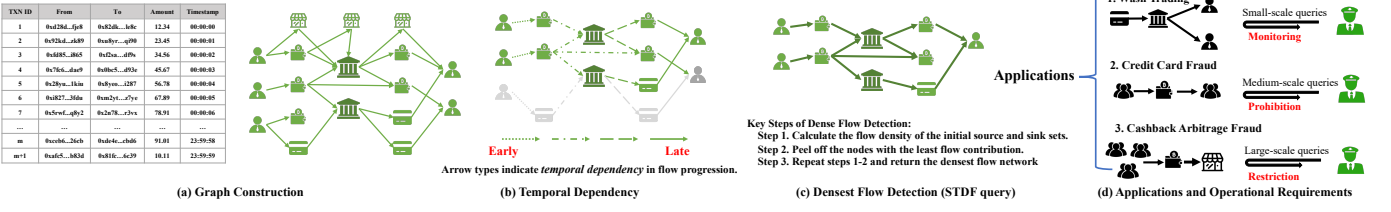


Fig. 1: Densest Flow Query on Transaction Flow Networks and Example Applications in Grab

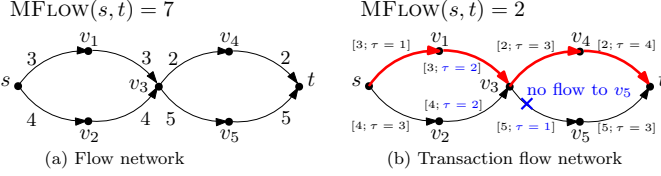


Fig. 2: A transaction flow network

the flow value represented by  $\text{MFLOW}(s, t)$ . To approach this problem, it is known that we can introduce a super source  $s'$ , connecting it to each source  $s_i \in S$  with an edge  $(s', s_i)$  of an infinite capacity  $C(s', s_i) = +\infty$ . Similarly, a super sink  $t'$  is created and linked to each sink  $t_i \in T$  via an edge  $(t_i, t')$ , with an infinite capacity  $C(t_i, t') = +\infty$ . This ensures that  $\text{MFLOW}(s', t') = \text{MFLOW}(S, T)$  [3].

Existing studies [37], [30], [54] overlook temporal dependency, which limits the effectiveness. Here, we extend the definitions to capture temporal dependency.

**Timestamp.** A transaction, represented as an edge, is naturally associated with an occurrence timestamp, denoted by  $\tau$ . Here,  $\tau$  indicates the chronological order of transactions, where larger values of  $\tau$  indicate more recent transactions. Then, Transaction Flow Network (TFN) is formalized as follows:

**Definition II.2 (TFN).** A TFN  $G = (V, E, C, \mathcal{T})$  is a directed graph where: (a)  $V$ ,  $E$ , and  $C$  retain their definitions from the flow network, and (b)  $\mathcal{T} : E \rightarrow \mathbb{Z}^+$  is a timestamp mapping function assigning a timestamp to each edge  $e = (u, v) \in E$ , indicating the moment the transaction occurred, denoted by  $\mathcal{T}(e)$  or  $\mathcal{T}(u, v)$ .

**Temporal flow.** In a TFN, a temporal flow from  $s$  to  $t$  is a standard flow that additionally respects *temporal dependency*: for every intermediate vertex  $u$  and every time  $\tau$ , the total amount of money that has *entered*  $u$  up to time  $\tau$  is at least the total amount that has *left*  $u$  by time  $\tau$ . Intuitively, an account cannot spend funds *before* it receives them.

Formally, we use the same capacity and flow-conservation conditions as in the static case, and enforce the above cumulative inout constraint at every vertex and time point. For brevity, we denote the maximum temporal flow value from  $s$  to  $t$  by  $\text{MFLOW}(s, t)$ . Figure 2 illustrates how the temporal constraint can drastically reduce the feasible flow compared to the static case.

**Example II.1.** Consider the network in Figure 2(a), the maximum flow value  $\text{MFLOW}(s, t) = 7$ . In Figure 2(b), each edge is annotated with a timestamp. Referring to Definition II.2, observe that no flow is permissible from  $v_1$  to  $v_5$  via  $v_3$  as the transaction from  $v_1$  to  $v_3$  occurs after the transaction from  $v_3$  to  $v_5$  ( $\mathcal{T}(v_1, v_3) > \mathcal{T}(v_3, v_5)$ ), thereby breaching the temporal

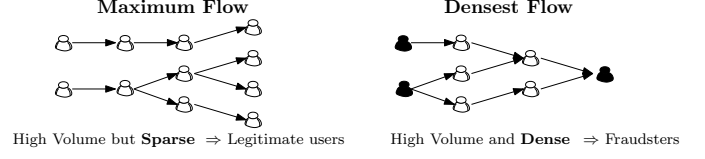


Fig. 3: Difference between Maximum Flow and Densest Flow  
*flow constraint at  $\tau = 1$ . A similar temporal discrepancy prevents flow from  $v_2$  to  $v_5$  through  $v_3$ . The only viable temporal flow paths from  $s$  to  $t$  are highlighted in red, resulting in a maximum temporal flow value,  $\text{MFLOW}(s, t) = 2$ .*

### B. Problem Statement

While many accounts with high-flow volumes, as depicted in Figure 3, may belong to legitimate institutions or active users, relying solely on maximum flow analysis is insufficient to distinguish fraudulent users from these legitimate entities. Previous studies have indicated that fraudulent activities often involve large-volume transfers within a small, concentrated group of participants, thereby creating a pattern of dense financial flows [43]. Such a pattern underscores the need for a more nuanced metric that captures not just the volume, but also the density of these flows.

**Flow Density.** Given a set of sources  $S$  and a set of sinks  $T$ , the flow density from  $S$  to  $T$  is defined as the maximum flow value divided by the sum of the sizes of  $S$  and  $T$  [37], [30], [54], specifically  $g(S, T) = \frac{\text{MFLOW}(S, T)}{|S|+|T|}$ .

**S-T Densest Flow (STDF).** Given a flow network  $G$ , a set  $S$  of sources, a set  $T$  of sinks, and an integer  $k$ , STDF is to find a subset  $S' \subseteq S$  and a subset  $T' \subseteq T$ , such that  $|S'|+|T'| \geq k$ , and maximize the flow density,  $g(S', T')$ .

**The STDF Decision Problem.** Given a flow network  $G$ , a set  $S$  of sources and a set  $T$  of sinks, and a parameter  $c$ , is there a subset  $S' \subseteq S$  and a subset  $T' \subseteq T$  such that  $|S'|+|T'| \geq k$  and  $g(S', T') \geq c$ ? The STDF decision problem is proven NP-complete in Lemma II.1, thus making the optimization problem of STDF NP-hard.

**Lemma II.1.** STDF decision problem is NP-complete.

*Proof. sketch.* The proof is based on a reduction from the decision problem of the densest at least  $k$  subgraph (DkS) (cf. [20]). The proof is presented in [2], due to space limitations.  $\square$

Building upon STDF and incorporating the temporal flow constraint, we introduce  $\mathcal{T}$ -STDF. Notably, STDF represents a particular case of  $\mathcal{T}$ -STDF, where the timestamp  $\tau$  for all edges in the TFN is set to 1.

**Problem Statement.** Given a TFN  $G = (V, E, C, \mathcal{T})$ , and a  $\mathcal{T}$ -STDF query  $Q = (S, T, k)$ , the answer of  $Q$ , denoted as

$Q(G) = (f, (S', T'))$  of  $Q$ , where  $S' \subseteq S$  and  $T' \subseteq T$  is a pair of proper subsets that maximizes the density  $g(S', T')$  on  $G$ , and  $f$  is the maximum flow from  $S'$  to  $T'$ . This paper aims to determine the answer of a given query,  $Q(G)$ .

### C. Modeling Rationale

**Flow-based density.** Unlike classical edge-density [37], [30], [54] measures that rely solely on the sum of edge weights, transaction networks naturally obey flow capacity, flow conservation, and temporal ordering constraints. Ignoring these constraints may treat non-executable or duplicated transfers as dense patterns. Using  $\text{MFLOW}(S, T)$  ensures that the detected density reflects the *actual realizable amount of money* transferable from  $S$  to  $T$ , which is essential for modeling money laundering chains, wash trading loops, and multi-hop smurfing structures observed in practice.

**Normalization choices.** A geometric-mean normalization such as  $\text{MFLOW}(S, T)/\sqrt{|S||T|}$  is mathematically dominated by the smaller of  $|S|$  and  $|T|$ , which artificially inflates the density of highly unbalanced groups a common pattern in fraud (e.g., few sources but many mule accounts). In contrast, the arithmetic term  $|S|+|T|$  penalizes the two sides proportionally, yielding a more stable and size-consistent measure that reflects the collective participation of all accounts. This linear scaling also aligns with prior fraud-detection formulations [37], [30], [54], making it appropriate for transaction-flow networks.

**Why a transaction-flow network (TFN) and compatibility with multilayer models.** Although real payment ecosystems may involve multiple operational layers (e.g., cards, wallets, merchants), industrial fraud-monitoring systems (including Grabs) standardize all records into a unified account-to-account transaction log. The TFN abstraction therefore preserves exactly the information required for computing temporal maximum flows. Importantly, our formulation is fully *compatible* with multilayer representations: a multilayer network can be flattened to a TFN by treating cross-layer edges as ordinary directed edges, or conversely, a TFN can be lifted to a multilayer model without affecting the temporal-flow constraints or the definition of the STDF objective. Thus, using a TFN does not restrict generality, while avoiding the additional semantic and computational complexity introduced by explicit multilayer models.

**Why  $S$  and  $T$  are not partitions.** In fraud scenarios,  $S$  and  $T$  represent accounts with net outgoing and net incoming behavior, respectively, rather than a graph bipartition. This directional interpretation is consistent with real fraudulent workflows (source  $\rightarrow$  mule layers  $\rightarrow$  sink), making it more appropriate than using  $(S, T)$  as a generic cut.

**Size constraints.** In fraud scenarios, the ratio between sources and sinks is highly unpredictable: a credit-card fraud case may have only a few sources but many receiving mule accounts, whereas cashback-arbitrage schemes may involve large and fluctuating groups on both sides. Because such proportions are unknown *a priori*, setting two independent thresholds ( $k_1, k_2$ ) is operationally impractical there is no reliable way for investigators to determine appropriate values. In contrast, a single size constraint  $|S'|+|T'| \geq k$  reflects the requirement that a fraud group must contain at least  $k$  participants while allowing

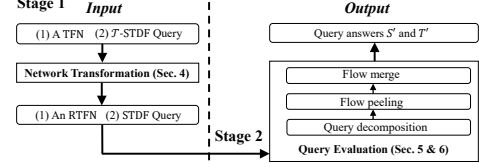


Fig. 4: A two-stage solution overview of Conan

the algorithm to automatically choose the most meaningful split between  $S'$  and  $T'$ . This makes the formulation practical across heterogeneous fraud types.

### III. SOLUTION OVERVIEW OF CONAN

To evaluate the  $\mathcal{T}$ -STDF query, we propose a two-stage solution called Conan (see Figure 4). Our solution is driven by practical industry insights from fraud detection at Grab.

**Observation 1.** Fraudulent activities exhibit temporal dependencies that differ from normal user behavior patterns. For example, in credit card fraud, fraudsters transfer funds following specific time sequences. Considering temporal dependencies increases detection accuracy from 64.93% to 82.39%.

**Stage 1: Network Transformation.** Conan comprises a lightweight network transformation technique for evaluating  $\mathcal{T}$ -STDF on the transformed networks, called RTFN (detailed in Section IV). This technique ensures the correctness of the maximum temporal flow and enables transforming the  $\mathcal{T}$ -STDF query into a STDF query (Figure 4). It is proven that any maximum flow algorithms can be applied (without modification) to the transformed network to obtain maximum temporal flows. The answers to the  $\mathcal{T}$ -STDF query can be simply derived from the RTFN and the answer to the corresponding STDF query.

**Observation 2.** In scenarios like cashback arbitrage fraud, transaction flows within certain groups are extremely dense. At Grab, executing a dense flow query can take several hours, delaying fraud detection and allowing fraudulent activities to continue undetected. Efficient algorithms are essential to process these dense flows promptly.

**Stage 2: Query Evaluation.** Given a STDF query,  $Q = (S, T, k)$ , Conan evaluates the query in a divide-and-conquer algorithm. Firstly, Conan divides  $S$  (resp.  $T$ ) into subsets  $S_i$  (resp.  $T_i$ ) (Section V-A). Then, Conan peels the vertices recursively in each  $S_i$  and  $T_i$  (Section VI). After finding the 3-approximate densest flows from  $S_i$  to  $T_i$ , Conan combines them to obtain the global 3-approximate densest flow.

### IV. BASELINE FOR MAXIMUM TEMPORAL FLOW

Existing work on maximum flow falls into two categories, neither of which applies to the STDF setting.

(1) *Classical static max-flow algorithms.* Algorithms such as augmenting-path methods [21], push-relabel [13], and pseudoflow [28] operate on static networks and rely on unrestricted flow reversal in the residual graph. Such reversal violates the temporal-dependency, and therefore these algorithms cannot compute correct temporal flows (cf. Fig. 5).

(2) *Temporal-flow formulations.* Prior temporal-flow studies are based on problem definitions fundamentally different from ours. Earliest-arrival and transit-time models [22], [63], [50],

[55] optimize arrival time under traversal delays and do not enforce the funds-must-arrive-before-they-can-leave causality constraint. Similarly, models with time-varying or ephemeral edge availability [27], [4] assume intermittent edge activation but do not require cumulative temporal feasibility at intermediate vertices. Our temporal flow, in contrast, requires monotone non-decreasing timestamps on any feasible augmenting path and regret-enabled flow reversal to preserve such causality-constraints absent from all prior formulations. Because these methods also operate only in the single-sourcesingle-sink, single-evaluation setting, they cannot be directly applied to STDF.

These limitations motivate our regret-enabled transformation, which converts a TFN into a static network that preserves temporal consistency and allows any high-performance max-flow algorithm to be used correctly.

**Residual Network.** Given a TFN  $G = (V, E, C, \mathcal{T})$  and a flow  $f$ , the residual network is denoted as  $G_f = (V_f, E_f, C_f, \mathcal{T}_f)$ . The residual capacities  $C_f$  and timestamps  $\mathcal{T}_f$  for  $(u, v) \in V \times V$  are defined as:

$$\langle C_f(u, v), \mathcal{T}_f(u, v) \rangle = \begin{cases} \langle C(u, v) - f(u, v), \mathcal{T}(u, v) \rangle & \text{if } (u, v) \in E \\ \langle f(v, u), \mathcal{T}(v, u) \rangle & \text{if } (v, u) \in E \\ \langle 0, 0 \rangle & \text{otherwise} \end{cases} \quad (1)$$

where  $V_f = V$  and  $E_f = \{(u, v) \mid C_f(u, v) > 0\}$ .

Given a TFN  $G = (V, E, C, \mathcal{T})$ , a source  $s$  and a sink  $t$ , a path  $P = (v_1, \dots, v_n)$  is a *temporal augmenting path* if a)  $v_1 = s$ ; b)  $v_n = t$ ; and c)  $\forall i \in [2, n-1], \mathcal{T}(v_{i-1}, v_i) \leq \mathcal{T}(v_i, v_{i+1})$ .

**Definition IV.1** (Regret-disabling vertex (RDV)). *In a TFN,  $G = (V, E, C, \mathcal{T})$ , a vertex  $u$  is designated as an RDV if  $\exists \tau_1, \tau_2 \in \mathcal{T}_u^{\text{in}}, \tau_3, \tau_4 \in \mathcal{T}_u^{\text{out}}$  such that  $\tau_1 < \tau_3 < \tau_2 < \tau_4$ , where (i)  $\mathcal{T}_u^{\text{in}} = \{\mathcal{T}(v, u) \mid (v, u) \in E\}$ , and (ii)  $\mathcal{T}_u^{\text{out}} = \{\mathcal{T}(u, v) \mid (u, v) \in E\}$ .*

The presence of RDVs in a TFN poses challenges for classic maximum flow algorithms. To illustrate this issue, we provide a brief example below.

**Example IV.1.** *In a TFN as depicted in Figure 5,  $\mathcal{T}(v_1, v_3) = 3$ ,  $\mathcal{T}(v_2, v_3) = 5$ ,  $\mathcal{T}(v_3, v_4) = 4$ , and  $\mathcal{T}(v_3, v_5) = 6$ .  $v_3$  is an RDV since  $\mathcal{T}(v_1, v_3) < \mathcal{T}(v_3, v_4) < \mathcal{T}(v_2, v_3) < \mathcal{T}(v_3, v_5)$ . Suppose that the first found temporal augmenting path is  $p_1 = (s, v_1, v_3, v_5, t)$  with a temporal flow value  $|f_1| = 5$ . The residual network after finding  $p_1$  results in a second temporal augmenting path,  $p_2$ , and the temporal flow value along  $p_2$  is  $|f_2| = 1$ . Thus, the value of temporal flow from  $s$  to  $t$  found by classic algorithms is only  $|f_1| + |f_2| = 6$  as shown in Figure 5(c). Due to the temporal flow constraint, it is not possible to flow from  $v_2$  to  $v_4$  through  $v_3$  (as shown in Figure 5(b)) unless part of  $f_1$  is reversed. An alternate augmenting path,  $p_1 = (s, v_1, v_3, v_4, t)$  must be selected at the beginning (as shown in Figure 5(a)). The maximum temporal flow from  $s$  to  $t$  of this TFN is  $\text{MFLOW}(s, t) = 8$  if three augmenting paths are found in the order of  $(s, v_1, v_3, v_4, t)$ ,  $(s, v_1, v_3, v_5, t)$ , and  $(s, v_2, v_3, v_5, t)$ . The residual network is shown in Figure 5(d).*

To resolve this issue, we present our TFN transformation that enables augmenting-path-based algorithms to compute the correct maximum flow value.

**Network Transformation Algorithm.** Given a TFN,  $G = (V, E, C, \mathcal{T})$ , Conan transforms  $G$  into a **Regret-enabled Temporal Flow Network (RTFN)**  $\widehat{G} = (\widehat{V}, \widehat{E}, \widehat{C})$  which is *regret-enabled* for classic maximum flow algorithms to reverse the flow identified in previous iterations. To accomplish this, Conan builds a *virtual* Cartesian coordinate system  $xOy$  with the vertices on the  $x$ -axis and the timestamps on the  $y$ -axis. The key steps, that run in  $O(|V|+|E|)$ , are as follows.

- 1) **Initialization.**  $\widehat{G}$  is initialized as an empty graph.
- 2) **Iterative steps.** For each edge  $e = (u, v)$  to be transformed, where  $\tau = \mathcal{T}(e)$ , a copy  $u^\tau$  of  $u$  (resp.  $v^\tau$  of  $v$ ) is created at the coordinate  $\langle u, \tau \rangle$  (resp.  $\langle v, \tau \rangle$ ) in the  $xOy$  Cartesian coordinate system. The edge  $e$  is transformed into  $\hat{e} = (u^\tau, v^\tau)$  with capacity  $\widehat{C}(\hat{e}) = C(e)$ . For all copies  $\{u^{\tau_1}, \dots, u^{\tau_k}\}$  of vertex  $u$ , additional edges  $e' = (u^{\tau_i}, u^{\tau_{i+1}})$  for  $i \in [1, k-1]$  are added to  $\widehat{G}$  with capacity  $\widehat{C}(e') = +\infty$ . To ease the discussion,  $\hat{e}$  is referred to as the "horizontal edge", while  $e'$  is referred to as the "vertical edge".
- 3) **Termination.** The transformation terminates when all vertices and edges have been transformed.

**Example IV.2.** Consider the TFN in Figure 5(a). The transformation is shown in Figure 6(a).  $\widehat{G}$  is initialized as an empty graph (Step (1)). The edge  $(s, v_1)$  of  $G$  is transformed into  $(s^1, v_1^1)$  of  $\widehat{G}$ . Consider the edge  $(v_1, v_3)$  in  $G$ , the vertices  $v_1^3$  and  $v_3^3$ , and the horizontal edge  $(v_1^3, v_3^3)$  are created in  $\widehat{G}$ . The existence of  $v_1^1$  also results in the addition of a vertical edge  $(v_1^1, v_1^3)$  to  $\widehat{G}$  (Step (2)). The RTFN shown in Figure 6(a) (Step (3)) is the network after all edges are transformed.

We establish in Theorem IV.1 that the maximum flow values in RTFN and TFN are identical. To avoid disrupting the presentation flow, we present its proof in [2]).

**Theorem IV.1.** *Given a TFN  $G$  with a source  $s$  and a sink  $t$ , the value of  $\text{MFLOW}(s, t) = \text{MFLOW}(s^{\tau_1}, t^{\tau_{\max}})$  in the RTFN  $\widehat{G}$ , where the earliest copy of a source  $s$  and the latest copy of a sink  $t$  as  $s^{\tau_1}$  and  $t^{\tau_{\max}}$ , respectively.*

We next illustrate that classic algorithms are applied on RTFN to compute the maximum temporal flow value.

**Example IV.3.** Consider RTFN in Figure 6 (a). Assume that the first augmenting path found is  $p_1$  with a temporal flow of  $|f_1| = 5$ . The second augmenting path found is  $p_2$  in the residual network  $G_{f_1}$  resulting in  $|f_2| = 2$ .  $p_2$  is found as there is a reverse edge  $(v_3^5, v_3^4)$  in  $G_{f_1}$  that enables the flow to be reversed. When the last augmenting path  $p_3$  with a temporal flow of  $|f_3| = 1$  is found, the maximum flow from  $s$  to  $t$  is computed by  $\text{MFLOW}(s, t) = |f_1| + |f_2| + |f_3| = 8$ .

**Remarks.** With Theorem IV.1, we assume that Conan transforms any source  $s_i \in S$  (resp. any sink  $t_i \in T$ ) in the  $\mathcal{T}$ -STDF query to  $s_i^{\tau_1}$  (resp.  $t_i^{\tau_{\max}}$ ) in the RTFN. We will focus on the STDF query on the RTFN for simplicity.

## V. DIVIDE-AND-CONQUER APPROACH

As presented in Section II-B, the density metric  $g(S, T)$  is defined as  $\frac{\text{MFLOW}(S, T)}{|S|+|T|}$ . It is evident that the maximum

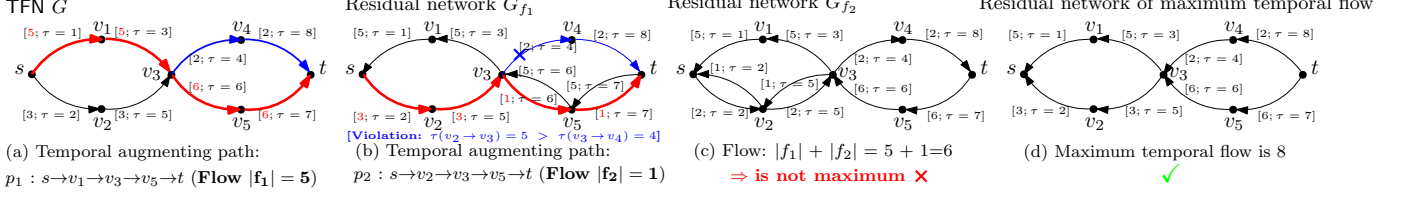


Fig. 5: (a)-(c) classic algorithms cannot return maximum temporal flow, and (d) Residual network of maximum temporal flow.

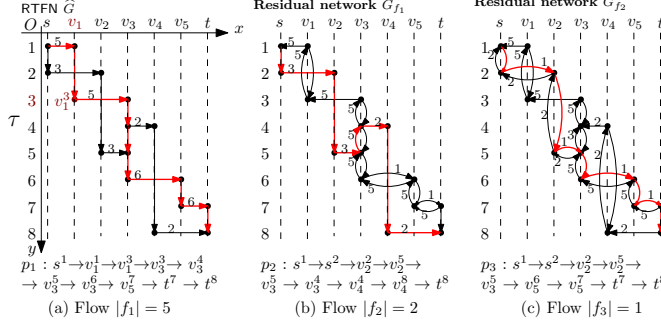


Fig. 6: (a) RTFN  $\widehat{G}$ , (a-c) three augmenting paths  $p_1$ ,  $p_2$  and  $p_3$ , and (b-c) two residual networks  $G_{f1}$  and  $G_{f2}$ . (Remarks: The capacity on vertical edges is  $+\infty$  unless specified.)

flow is the densest when  $|S|+|T|$  is fixed. However, it is time-consuming to enumerate all possible subsets of  $S$  and  $T$  and compute the maximum flows to answer the STDF queries  $Q = (S, T, k)$  since this approach would require computing the maximum flow  $2^{|S|+|T|}$  times. Hence, we propose an efficient divide-and-conquer approach to reduce the number of maximum flow computations. Specifically, given a query  $Q = (S, T, k)$ , Conan decomposes  $S$  and  $T$  into smaller subsets (Section V-A), finds densest flows for each fixed  $|S'|+|T'|$  for each pair of subsets (Section V-B), and merges the densest flows to answer the query that  $|S'|+|T'| \geq k$  (Section V-C).

#### A. Query Decomposition

In this subsection, we propose to decompose the query subsets  $S$  and  $T$  into smaller, non-overlapping subsets  $S_i$  and  $T_i$ . We first present how to determine these subsets.

**Reachability.** Given a source  $s$  and a sink  $t$ , if there is a path from  $s$  to  $t$ , we say  $s$  can reach  $t$  and denote the reachability by  $\text{REACH}(s, t) = \text{True}$ . Otherwise,  $\text{REACH}(s, t) = \text{False}$ .

**Overlap of Flows.** Given two pairs of a source and a sink  $(s_1, t_1)$  and  $(s_2, t_2)$ , if  $\text{REACH}(s_1, t_1) = \text{False}$  and  $\text{REACH}(s_2, t_1) = \text{False}$ , the flows  $f_1$  and  $f_2$  are *overlap-free*, where  $f_1$  (resp.  $f_2$ ) is the flow from  $s_1$  (resp.  $s_2$ ) to  $t_1$  (resp.  $t_2$ ). Otherwise,  $f_1$  and  $f_2$  overlap. We have the following property if two flows are overlap-free.

**Property 1.** Given two pairs  $(s_1, t_1)$  and  $(s_2, t_2)$ , and their maximum flow values  $|f_1| = \text{MFLOW}(s_1, t_1)$  and  $|f_2| = \text{MFLOW}(s_2, t_2)$ . If the flows  $f_1$  and  $f_2$  are overlap-free,  $|f_1| + |f_2| = \text{MFLOW}(\{s_1, s_2\}, \{t_1, t_2\})$ .

**Vertex Set Decomposition.** With Property 1, Conan divides the queries based on the reachability between the sources  $S$ , and the sinks  $T$ , into subset pairs, denoted by  $\text{WCC}_i = (S_i, T_i)$  ( $i \in [1, \text{nw}]$ ), where  $\text{nw}$  is the number of subset pairs. The sources in  $S_i$  and the sinks in  $T_i$  are located within the same

weakly connected component (WCC). We remark that the sources (resp. sinks) outside the WCC are not reachable to  $T_i$  (resp. from  $S_i$ ). The decomposition satisfies the following:

- 1)  $S = \bigcup_{i \in [1, \text{nw}]} S_i$  and  $T = \bigcup_{i \in [1, \text{nw}]} T_i$ ; and
- 2)  $\forall i, j \in [1, \text{nw}]$ ,  $S_i \cap S_j = \emptyset$ , and  $T_i \cap T_j = \emptyset$ .

If  $(S_1, T_1)$  and  $(S_2, T_2)$  are two distinct WCCs, the maximum flows  $f_1$  and  $f_2$  must be overlap-free, where  $f_1$  (resp.  $f_2$ ) is the maximum flow from  $S_1$  (resp.  $S_2$ ) to  $T_1$  (resp.  $T_2$ ). Otherwise,  $f_1$  and  $f_2$  overlap.

**Property 2.** Given two maximum flows,  $f_1$  from  $S_1$  to  $T_1$  and  $f_2$  from  $S_2$  to  $T_2$ , if  $f_1$  and  $f_2$  are overlap-free,  $\text{MFLOW}(\{S_1, S_2\}, \{T_1, T_2\}) = |f_1| + |f_2|$ .

**Example V.1.** Given a query  $Q = (S, T, 4)$  shown in Figure 7, where  $S = \{s_1, s_2, s_3, s_4\}$  and  $T = \{t_1, t_2, t_3, t_4, t_5\}$ , there are  $2^{|S|+|T|} = 512$  combinations, i.e., 512 times maximum flow calculations. By checking the reachability, we obtain two WCCs:  $\text{WCC}_1 = (S_1, T_1)$ , where  $S_1 = \{s_1, s_2\}$  and  $T_1 = \{t_1, t_2, t_3\}$ , and  $\text{WCC}_2 = (S_2, T_2)$ , where  $S_2 = \{s_3, s_4\}$  and  $T_1 = \{t_4, t_5\}$ , as shown in Figure 7(a). There are  $2^{|S_1|+|T_1|} = 32$  (resp.  $2^{|S_2|+|T_2|} = 16$ ) combinations on  $\text{WCC}_1$  (resp.  $\text{WCC}_2$ ). Thus, a total of  $32 + 16 = 48$  maximum flow calculations are needed, which is only 9.4% of the calculations required by directly enumerating subsets of  $S$  and  $T$ .

#### B. Computing Intermediate Densest Flows

We compute and store intermediate densest-flow values in a *densest-flow (DF) array*, denoted  $\text{DF}_i$ . For each  $\text{WCC}_i = (S_i, T_i)$ ,  $i \in [1, \text{nw}]$ ,  $\text{DF}_i[k] = \text{MFLOW}(S', T')$  which is the densest flow value from  $S' \subseteq S_i$  to  $T' \subseteq T_i$ , such that  $|S'| + |T'| = k$  and  $g(S', T')$  is maximized. The length of  $\text{DF}_i$ , denoted as  $\text{len}(\text{DF}_i)$ , is  $|S_i| + |T_i| + 1$  since  $0 \leq k \leq |S_i| + |T_i|$ . All the arrays,  $\text{DF}_i$ s, are stored in a sequence  $\text{DF}$ .

**Example V.2.** Consider  $\text{WCC}_1 = (S_1, T_1)$  in Example V.1.  $\text{DF}_1$  is initialized with a length of 5. For  $k = 3$ , the flow from  $S' = \{s_2\}$  to  $T' = \{t_2, t_3\}$  is the densest with the flow value  $\text{DF}_1[3] = \text{MFLOW}(S', T') = 9$ . Similarly,  $\text{DF}_1[2] = 5$  with  $S' = \{s_2\}$  and  $T' = \{t_2\}$ ,  $\text{DF}_1[4] = 10$  with  $S' = \{s_1, s_2\}$  and  $T' = \{t_2, t_3\}$ , and  $\text{DF}_1[5] = 11$  with  $S' = \{s_1, s_2\}$  and  $T' = \{t_1, t_2, t_3\}$ .  $\text{DF}_2$  for  $\text{WCC}_2$  is shown in Figure 7(b).

**Time Complexity.** The state-of-the-art indexes e.g., [38], [39], [12], [58] can be used to determine the reachability between the sources  $S$  and the sinks  $T$ . WCCs can be found in  $O(|S||T|\log|V|)$  by using these indexes. The time complexity to compute the densest flow arrays,  $\text{DF}_i$  for  $i \in [1, \text{nw}]$ , is  $O(\sum_{i=1}^{\text{nw}} 2^{|S_i|+|T_i|} M)$ , where  $M$  is the complexity of any maximum flow algorithms.

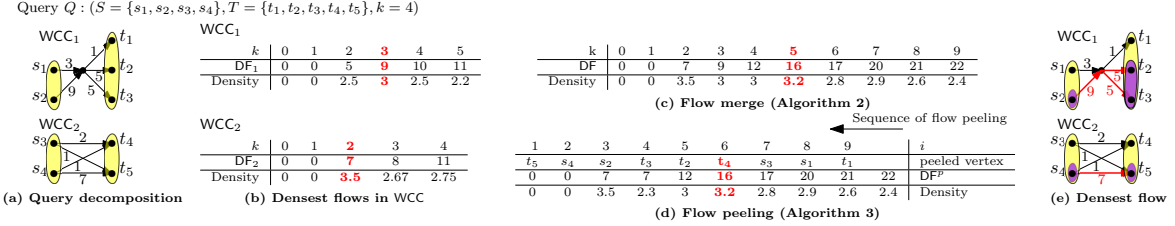


Fig. 7: STDF evaluation (A running example)

**Algorithm 1:** Densest Flow Merge

```

Input: A sequence of densest flow arrays  $\mathbf{DF} = [\mathbf{DF}_1, \dots, \mathbf{DF}_{\text{nw}}]$ 
Output: A merged densest flow array  $\mathbf{DF}'$ 
1 return  $\text{DFM}(\mathbf{DF}, 1, \text{nw})$ 
2 Function  $\text{DFM}(\mathbf{DF}, l, r)$ 
3   if  $l = r$  then // only one densest flow array
4     return  $\mathbf{DF}_l$ 
5    $m \leftarrow \lfloor \frac{l+r}{2} \rfloor$ 
6   return  $\text{ARRMRG}(\text{DFM}(\mathbf{DF}, l, m), \text{DFM}(\mathbf{DF}, m+1, r))$ 
7 Function  $\text{ARRMRG}(\mathbf{DF}_1, \mathbf{DF}_2)$ 
8   init an empty densest flow array  $\mathbf{DF}'$ 
9   foreach  $k \in [0, \dots, \text{len}(\mathbf{DF}_1) + \text{len}(\mathbf{DF}_2) - 1]$  do
10    |  $\mathbf{DF}'[k] \leftarrow 0$ 
11   foreach  $k_1 \in [0, \dots, \text{len}(\mathbf{DF}_1) - 1]$  do
12    | foreach  $k_2 \in [0, \dots, \text{len}(\mathbf{DF}_2) - 1]$  do
13    |   | if  $\mathbf{DF}'[k_1 + k_2] < \mathbf{DF}_1[k_1] + \mathbf{DF}_2[k_2]$  then
14    |   |   |  $\mathbf{DF}'[k_1 + k_2] \leftarrow \mathbf{DF}_1[k_1] + \mathbf{DF}_2[k_2]$ 
15 return  $\mathbf{DF}'$ 

```

**C. Merging of Intermediate Densest Flows**

We next propose an efficient method for merging the densest flow of each WCC to yield the global densest flow array for solving STDF. We prove in Lemma V.1 that the densest flow of multiple WCCs can be constructed from the densest flows of individual WCCs.

**Lemma V.1.** Given  $\text{WCC}_i = (S_i, T_i)$  and  $\text{WCC}_j = (S_j, T_j)$ , if  $S'_i \subseteq S_i$ ,  $T'_i \subseteq T_i$ ,  $S'_j \subseteq S_j$ , and  $T'_j \subseteq T_j$ , then

$$\text{MFLOW}(S'_i \cup S'_j, T'_i \cup T'_j) = \text{MFLOW}(S'_i, T'_i) + \text{MFLOW}(S'_j, T'_j). \quad (2)$$

Algorithm 1 of Conan merges the densest flow arrays,  $\mathbf{DF}$ , in a recursive manner (Line 1 and Lines 2-6). If there is only one array to be merged, it is returned directly (Line 4). If there are two arrays to be merged (Line 7), Conan first initializes an array  $\mathbf{DF}'$  to store the merged densest flow (Line 8). Conan compares  $\mathbf{DF}_1[k_1] + \mathbf{DF}_2[k_2]$  with  $\mathbf{DF}[k_1 + k_2]$  ( $k_1 \in [0, \text{len}(\mathbf{DF}_1)]$ ,  $k_2 \in [0, \text{len}(\mathbf{DF}_2)]$ ) by iterating through  $\mathbf{DF}_1$  and  $\mathbf{DF}_2$ . If  $\mathbf{DF}_1[k_1] + \mathbf{DF}_2[k_2]$  is greater than  $\mathbf{DF}[k_1 + k_2]$ , a denser flow is found (Line 14). If there are more than two densest flow arrays, they are divided into two parts and merged recursively (Line 6). Once all  $\mathbf{DF}$ s have been merged, a global densest flow array  $\mathbf{DF}$  is obtained and returned (Line 1).

**Computing the Answer of STDF from  $\mathbf{DF}$ .** For a STDF query,  $Q = (S, T, k)$ , the maximal value of  $\frac{\mathbf{DF}[k']}{k'}$  is returned, where  $k' \geq k$ . The subsets  $S'$  and  $T'$  can be obtained using an inverted map. The implementation details are omitted due to space limitations.

**Example V.3.** For WCCs in Example V.1, their densest flow arrays are  $\mathbf{DF}_1 = [0, 5, 9, 10, 11]$  and  $\mathbf{DF}_2 = [0, 7, 8, 11]$  (Figure 7(b)). Consider the merged densest flow  $\mathbf{DF}[5]$ . There are 5 pairs of  $k_1$  and  $k_2$  such that  $k_1 + k_2 = 5$ . When  $k_1 = 3$  and  $k_2 = 2$ ,  $\mathbf{DF}[5] = \mathbf{DF}_1[3] + \mathbf{DF}_2[2] = 16$  is maximized. The rest elements in  $\mathbf{DF}$  are computed similarly

(Figure 7(c)). Consider the query  $Q = (S, T, 4)$  in Example V.1,  $\frac{\mathbf{DF}[5]}{5}$  is maximal. Therefore, the subsets  $S' = \{s_2, s_4\}$  and  $T' = \{t_2, t_3, t_5\}$  have the densest flow which consists of two sub-flows: 1) from  $\{s_2\}$  to  $\{t_2, t_3\}$ ; and 2) from  $\{s_4\}$  to  $\{t_5\}$  (Figure 7(e)). The answer to the query,  $Q$ , is  $S'$  and  $T'$  with a flow density of 3.2.

**Time Complexity.** Algorithm 1 has the time complexity of  $O((|S|+|T|)^2)$ . Specifically, the cost is

$$\sum_{i=2}^{\text{nw}} (\text{len}(\mathbf{DF}_i) \sum_{j=1}^i \text{len}(\mathbf{DF}_j)) < \sum_{i=1}^{\text{nw}} (\text{len}(\mathbf{DF}_i) \sum_{j=1}^{\text{nw}} \text{len}(\mathbf{DF}_j))$$

Since  $\sum_{j=1}^{\text{nw}} \text{len}(\mathbf{DF}_j) = |S|+|T|$ , the time complexity is bounded by  $O((|S|+|T|)^2)$ .

**VI. 3-APPROXIMATION ALGORITHM FOR STDF**

The divide-and-conquer approach (presented in Section V) solves the STDF query by dividing  $S$  and  $T$  into smaller subsets. However, when the subsets remain large, computing their densest-flow arrays is still expensive. Inspired by DkS [20], in Section VI-A we propose an approximate *flow peeling* algorithm with a one-third approximation guarantee to substantially reduce this cost. Section VI-B further introduces a pruning technique that reduces the number of maximum-flow computations.

**A. Flow Peeling Algorithm for STDF**

We use the term  $\text{PF}(u, S, T)$  to denote the reduction in the maximum flow value  $\text{MFLOW}(S, T)$  when vertex  $u$  is removed from the set  $S \cup T$ . This represents the *peeling flow* of vertex  $u$ .

**Definition VI.1** (Peeling Flow ( $\text{PF}$ )). Given a flow network  $G = (V, E, C)$ , a set  $S$  of sources and a set  $T$  of sinks,  $\text{PF}(u, S, T)$  is:

$$\text{PF}(u, S, T) = \begin{cases} \text{MFLOW}(S, T) - \text{MFLOW}(S \setminus \{u\}, T), & \text{if } u \in S \\ \text{MFLOW}(S, T) - \text{MFLOW}(S, T \setminus \{u\}), & \text{if } u \in T \end{cases} \quad (3)$$

**Flow Peeling (Algorithm 2, Figure 7(d)).** At the beginning of the flow peeling algorithm,  $S_n$  and  $T_n$  are set to  $S$  and  $T$ , respectively, and  $n$  is set to  $|S|+|T|$  (Lines 1). We use  $(S_i, T_i)$  to denote the vertex set pair after the  $i$ -th peeling step. The algorithm iteratively peels a vertex  $u_i$  either from  $S_i$  or  $T_i$  such that  $\text{PF}(u_i)$  is minimized (Lines 5-9). The process is repeated until all vertices have been peeled, resulting in a series of sets, denoted by  $(S_n, T_n), \dots, (S_0, T_0)$  of sizes  $n, \dots, 0$ . Then,  $S_i$  and  $T_i$  ( $i \in [k, n]$ ), that maximize the density metric  $g(S_i, T_i)$ , are returned. For simplicity, we denote the minimum peeling flow value in each step as  $\delta_i = \min\{\text{PF}(u_i, S_i, T_i) | u_i \in S_i \cup T_i\}$ .

**Example VI.1.** Consider the query  $Q$  in Example V.1. Figure 7(d) shows the full sequence of the flow peeling. Figure 8 shows the details of the flow peeling process when  $i = 6$

**Algorithm 2:** Flow Peeling Algorithm for STDF

---

**Input:**  $G = (V, E, C)$ ,  $Q = (S, T, k)$   
**Output:**  $Q(G)$

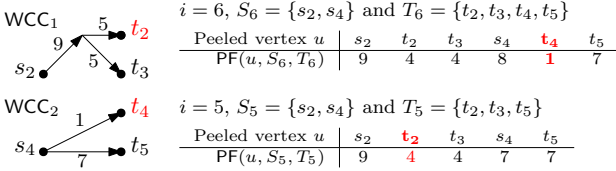
---

```

1  $n \leftarrow |S| + |T|$ ,  $S_n \leftarrow S$ ,  $T_n \leftarrow T$ 
2 foreach  $i \in [n-1, \dots, 0]$  do
3   |  $S_i \leftarrow \emptyset$ ,  $T_i \leftarrow \emptyset$ 
4 foreach  $i \in [n, \dots, 1]$  do
5   |  $\delta_i \leftarrow +\infty$  // init the minimum peeling flow
      | value
6   | foreach  $u \in S_i \cup T_i$  do // search for  $u$  minimizing
      |  $\text{PF}(u, S_i, T_i)$ 
7   |   | if  $\text{PF}(u, S_i, T_i) < \delta_i$  then
8   |   |   |  $\delta_i \leftarrow \text{PF}(u, S_i, T_i)$ 
9   |   |   |  $u_i \leftarrow u$ 
10  |   | if  $u_i \in S_i$  then // peel  $u_i$  from  $S_i$ 
11  |   |   |  $S_{i-1} \leftarrow S_i \setminus \{u_i\}$ ,  $T_{i-1} \leftarrow T_i$ 
12  |   | else // peel  $u_i$  from  $T_i$ 
13  |   |   |  $S_{i-1} \leftarrow S_i$ ,  $T_{i-1} \leftarrow T_i \setminus \{u_i\}$ 
14 return  $S_i$  and  $T_i$  maximizing density  $g(S_i, T_i)$ , where  $i \geq k$ 

```

---



and  $i = 5$ . When  $i > 6$ , vertices  $t_1$ ,  $s_1$  and  $s_3$  have been peeled. Therefore, when  $i = 6$ ,  $S_6 = \{s_2, s_4\}$  and  $T_6 = \{t_2, t_3, t_4, t_5\}$ . Since  $t_4$  has the smallest peeling flow value  $\text{PF}(t_4, S_6, T_6) = 1$ , it is peeled. This leaves  $S_5 = S_6 = \{s_2, s_4\}$  and  $T_5 = T_6 \setminus \{t_4\} = \{t_2, t_3, t_5\}$ . When  $i = 5$ ,  $t_2$  is peeled since it has the smallest peeling flow value. After all vertices are peeled, the returned sets  $(S_5, T_5)$  have the densest flow among all  $(S_i, T_i)$  ( $i \in [0, 9]$ ).

**Analysis of Approximation Ratio.** Due to space limitations, we only present the main ideas of the proofs. Detailed proofs of all lemmas and theorem are provided in [2].

To gain insights into the structural characteristics of networks and determine the essential vertices, we first present a definition of the *FCore*.

**Definition VI.2 (FCore).** Given a set  $S$  of sources and a set  $T$  of sinks,  $S^F \subseteq S$  and  $T^F \subseteq T$ , is an *FCore* if  $\forall u \in S^F \cup T^F$ ,  $\text{PF}(u, S^F, T^F) \geq F$ , denoted by  $(S^F, T^F) = \text{FCore}(S, T)$ .

Intuitively, vertices in  $\text{FCore}(S, T)$  have significant  $\text{PF}_s$  w.r.t.  $S$  and  $T$ . We can prove that *FCore* exists for  $0 \leq F \leq g(S, T)$ , where  $g(S, T)$  represents the density of the maximum flow from  $S$  to  $T$ .

**Lemma VI.1.** For any  $F \in [0, g(S, T)]$ , there always exists  $i \in [0, n]$  that  $(S_i, T_i) = \text{FCore}(S, T)$ .

For  $F \in [0, g(S, T)]$ , there may exist multiple *FCore*s. In the following, we focus on the *FCore* with the highest index  $i$  for  $S_i$  and  $T_i$ , i.e.,  $\delta_j < F$  for  $j \in (i, n]$ .

**Lemma VI.2.**  $\forall \alpha \in [0, 1]$  and  $F = \alpha \cdot g(S, T)$ ,  $(1 - \alpha) \text{MFLOW}(S, T) \leq \text{MFLOW}(S^F, T^F)$ .

Denote the exact answer to STDF query by  $(S', T')$ , consider  $\alpha = \frac{2}{3}$  and  $F = \alpha \cdot g(S, T)$ . Lemma VI.1 guarantees that there always exists  $(S_i, T_i)$  that is a *FCore*, and Lemma VI.2

**Algorithm 3:** Peeling Algorithms with Pruning

---

**Input:**  $G = (V, E)$ ,  $Q = (S, T, k)$   
**Output:**  $Q(G)$

---

```

1  $n \leftarrow |S| + |T|$ ,  $S_n \leftarrow S$ ,  $T_n \leftarrow T$ 
2 foreach  $i \in [n-1, \dots, 0]$  do
3   |  $S_i \leftarrow \emptyset$ ,  $T_i \leftarrow \emptyset$ 
4 foreach  $u \in S \cup T$  do
5   |  $\text{LPF}(u) = 0$  // Property 3
6 foreach  $i \in [n, \dots, 1]$  do
7   |  $\delta_i \leftarrow +\infty$ 
8   | Sort  $u \in S_i \cup T_i$  in the ascending order of  $\text{LPF}(u)$ 
9   | foreach  $u \in S_i \cup T_i$  do
10  |   | if  $\delta_i \leq \text{LPF}(u)$  then // early pruning
11  |   |   | break
12  |   | if  $\text{PF}(u, S_i, T_i) < \delta_i$  then
13  |   |   |  $\text{LPF}(u) \leftarrow \text{PF}(u, S_i, T_i)$ 
14  |   |   |  $\delta_i \leftarrow \text{PF}(u, S_i, T_i)$ 
15  |   |   |  $u_i \leftarrow u$ 
16  | if  $u_i \in S_i$  then
17  |   | foreach  $t \in T_i$  do // Property 4
18  |   |   |  $\text{LPF}(t) \leftarrow \text{LPF}(t) - \text{PF}(u, S_i, T_i)$ 
19  |   |   |  $S_{i-1} \leftarrow S_i \setminus \{u_i\}$ 
20  | else
21  |   | foreach  $s \in S_i$  do // Property 4
22  |   |   |  $\text{LPF}(s) \leftarrow \text{LPF}(s) - \text{PF}(u, S_i, T_i)$ 
23  |   |   |  $T_{i-1} \leftarrow T_i \setminus \{u_i\}$ 
24  |  $\delta_i \leftarrow \text{MFLOW}(S_i, T_i) - \text{MFLOW}(S_{i-1}, T_{i-1})$ 
25 return  $S_i$  and  $T_i$  maximizing density  $g(S_i, T_i)$ , where  $i \geq k$ 

```

---

guarantees that either  $(S_i, T_i)$  or  $(S_k, T_k)$  is a 3-approximation of the exact answer. Therefore, we have the following theorem.

**Theorem VI.3.** Algorithm 2 is a 3-approximation for STDF.

**Time Complexity.** Algorithm 2 requires  $|S| + |T|$  times the cost of the maximum flow calculation to obtain the smallest peeling flow for each  $i$ . Since there are at most  $|S| + |T|$  peelings, the time complexity is bounded by  $O((|S| + |T|)^2 M)$ , where  $M$  represents the complexity of any maximum flow algorithm.

**Remarks on the relation to DkS.** Although our flow-peeling procedure is conceptually inspired by the intuition behind DkS removing low-contribution vertices iteratively, the process of STDF is fundamentally different. In DkS, the marginal gain of a vertex is a *local*, additive quantity derived from edge weights, which enables classical degree-based peeling. In contrast, the marginal gain in STDF depends on a *global* multi-source multi-sink *temporal* maximum flow: removing one vertex may reroute, diminish, or eliminate entire flow paths, and its contribution cannot be inferred from local connectivity. Moreover, DkS is a special case of STDF obtained when all timestamps equal 1 and the flow value  $\text{MFLOW}(S, T)$  degenerates into the total edge weight between  $S$  and  $T$ . Because temporal flow interactions are non-decomposable, classical DkS peeling rules cannot be directly applied; thus, we introduce a new flow-based marginal definition and a flow-aware *FCore* ordering for STDF.

**B. Pruning in the Flow Peeling Algorithm**

Algorithm 2 enumerates all vertices  $s \in S_i$  (resp.  $t \in T_i$ ) and computes  $\text{MFLOW}(S_i \setminus \{s\}, T_i)$  (resp.  $\text{MFLOW}(S_i, T_i \setminus \{t\})$ ) in order to find the vertex  $u_i$  that minimizes the peeling flow  $\text{PF}(u, S_{i-1}, T_{i-1})$  (Line 9). However, this full enumeration is computationally expensive because each candidate requires a new maximum-flow evaluation.

To make this step more efficient, we exploit that peeling-flow values at later iterations are *algebraically constrained* by

WCC <sub>1</sub>				WCC <sub>2</sub>			
$s_2$	$t_3$	$t_2$	$s_1$	$t_5$	$s_4$	$t_4$	$s_3$
0	0	5	<b>9</b>	10	11	<b>7</b>	8
0	2.5	<b>3</b>	2.5	2.2	2.75	<b>3.5</b>	2.67
Density				$\text{DF}_1^P$			

(a) Densest flows in WCC by peeling

$k$	0	1	2	3	4	<b>5</b>	6	7	8	9
$\text{DF}^P$	0	0	7	7	12	<b>16</b>	17	20	21	22
Density	0	0	3.5	2.3	3	<b>3.2</b>	2.8	2.9	2.6	2.4

(b) Flow merge

Fig. 9: Examples of the divide-and-conquer peeling algorithm

those computed on larger source/sink sets: once  $\text{PF}(s, S, T)$  and  $\text{PF}(t, S, T)$  are known, the peeling flows after removing  $s$  or  $t$  cannot become arbitrarily small. This enables us to maintain, for every vertex  $u \in S \cup T$ , a *lower bound*  $\text{LPF}(u)$  on its future peeling-flow value without performing any max-flow computation. Intuitively, if the smallest already-computed peeling flow is strictly smaller than the minimum possible  $\text{LPF}$  among all remaining vertices, then no unexamined vertex can become the best peeling candidate, and the enumeration can be safely terminated. Based on this idea, we derive a set of properties that yield valid lower bounds for pruning unnecessary candidates.

**Property 3.**  $\forall u \in S \cup T, \text{PF}(u, S, T) \geq 0$ .

**Property 4.**  $\forall s \in S, t \in T,$

$$1) \text{PF}(t, S \setminus \{s\}, T) \geq \text{PF}(t, S, T) - \text{PF}(s, S, T); \text{ and} \quad (4)$$

$$2) \text{PF}(s, S, T \setminus \{t\}) \geq \text{PF}(s, S, T) - \text{PF}(t, S, T). \quad (5)$$

**Flow Peeling Using a Lower Bound (Algorithm 3).** By using Properties 3-4, we maintain a *lower bound* of the peeling flow for each vertex in  $S \cup T$ , denoted by  $\text{LPF}(u)$  (Line 5). To determine  $u_i$  that minimizes  $\text{PF}(u, S_{i-1}, T_{i-1})$ , we calculate  $\text{PF}(u)$ , where  $u \in S_i \cup T_i$ , in ascending order of  $\text{LPF}(u)$ . If the current minimum  $\text{PF}(u, S_i, T_i)$  is smaller than the minimum  $\text{LPF}$  of all vertices that have not been enumerated, the enumeration is terminated (Line 11), and  $u$  is chosen for the peeling.  $\text{LPF}(u)$  is refined if the following conditions are satisfied.

- 1) When  $\text{PF}(u, S_i, T_i)$  is calculated,  $\text{LPF}(u)$  is refined by  $\text{LPF}(u) = \text{PF}(u, S_i, T_i)$  (Line 13).
- 2) When a vertex  $u$  is peeled (Lines 16-23), if  $u \in S_i$ ,  $\text{LPF}(t)$  is refined by  $\text{LPF}(t) = \text{LPF}(t) - \text{PF}(u, S_i, T_i)$ , where  $t \in T_i$ ; otherwise,  $\text{LPF}(s)$  is refined by  $\text{LPF}(s) = \text{LPF}(s) - \text{PF}(u, S_i, T_i)$ , where  $t \in S_i$ .

**Time Complexity.** The time complexity of Algorithm 3 is  $O((|S|+|T|)^2 M)$ , where  $M$  is the complexity of any maximum flow algorithm. Sorting  $\text{LPFs}$  adds an extra  $O((|S|+|T|)^2 \cdot \log(|S|+|T|))$  cost. Since  $|S| \ll |V|$  and  $|T| \ll |V|$ , the sorting is efficient in practice. The pruning technique reduces the elapsed time of the peeling algorithm by avoiding enumerations and provides an approximation guarantee.

### C. Divide-and-conquer Peeling Algorithm

The flow peeling algorithm in Sections VI-A-VI-B is orthogonal to the divide-and-conquer approach (Section V). We propose to integrate them to obtain a divide-and-conquer peeling algorithm as follows.

- 1) **Query Decomposition.** Conan decomposes  $S$  and  $T$  into a set of WCCs as introduced in Section V-A.

- 2) **Flow Peeling.** Conan performs flow peeling on each  $\text{WCC}_i$  to produce the densest flow array, denoted by  $\text{DF}_i^P$ .
- 3) **Densest Flow Merge.** Conan merges  $\text{DF}_i^P$  to obtain the global answer of STDF by using Algorithm 1.

**Example VI.2.** In Figure 7, the sources and sinks are decomposed into two WCCs as depicted in Figure 7(a). Upon applying the peeling algorithms on each of these WCCs, two densest flow arrays ( $\text{DF}_1^P$  and  $\text{DF}_2^P$ ) are obtained as shown in Figure 9(a). Finally, these two densest arrays are merged to produce the global densest flow array  $\text{DF}^P$  (Figure 9(b)).

**Time Complexity.** The overall time complexity is  $O(\sum_{i=1}^{\text{nw}} (|S_i|+|T_i|)^2 M)$ , bounded by  $O((|S|+|T|)^2 M)$ , where  $M$  represents the complexity of any maximum flow algorithm.

**Space Complexity.** The sizes of both the original graph and the transformed graph are bounded by  $O(|V|+|E|)$ . The size of the flow array is bounded by  $O(|S|+|T|)$ .

## VII. EXPERIMENTAL STUDY

### A. Experimental Setup

**Software and Hardware.** Our experiments are conducted on a machine with a Xeon Gold 6330 CPU, and 64GB memory. The algorithms are implemented in C++ and the implementation is made memory-resident. All codes are compiled by GCC-8.5.0 with  $-O3$ . For computing the maximum flow, we implemented the algorithm from [18] as a built-in component. It should be remarked that any maximum flow algorithm could be employed to replace the one from [18].

**Datasets.** Our experiments are conducted on six datasets, including five real-world transaction-flow datasets and one large-scale synthetic benchmark.

- 1) Three real-world datasets are extracted from the Bitcoin transaction network in 2011, 2012, and 2013 [53]. In addition, we collect transactions from the Ethereum network in 2016 and 2021 [64]. We extract datasets by year because both the graph structure and transaction amount distributions vary significantly across time. In the early years, both BTC and ETH exhibit larger transaction values and denser activity.
- 2) To complement real-world data with a controllable benchmark, we additionally include the IBM synthetic transaction dataset released by the Watson Research Lab [5]. This dataset is designed to simulate realistic financial transaction flows at scale.

**Timespan.** We provide an interface that allows investigators to specify a detection timespan  $\Delta = [\tau_s, \tau_e]$ . For the real-world Bitcoin and Ethereum datasets, we evaluate Conan using three timespan lengthsone day, one week, and one monthdenoted by  $\Delta_d$ ,  $\Delta_w$ , and  $\Delta_m$ , respectively, which reflect common investigation practices on recent transactions. To generate queries, we randomly select 20 timespans from each type of time window for evaluation. For the IBM synthetic transaction dataset, we evaluate Conan on the full graph, since its timestamps are synthetically generated and do not correspond to operational investigation windows; this setting is sufficient for assessing scalability.

TABLE I: Statistics of datasets and queries of  $S$  and  $T$  with the default size  $n = 32$ , where  $\widehat{V}$  (resp.  $\widehat{E}$ ) denotes the vertex set (resp. edge set) of the compressed RTFN, and  $\Delta_d$  (resp.  $\Delta_w$  and  $\Delta_m$ ) denotes a time span of a day (resp. a week and a month)

Datasets	$V$	$E$	avg. $ \widehat{V} $ of the RTFN			avg. $ \widehat{E} $ of the RTFN			avg. out-degree of the vertices in $S$			avg. in-degree of the vertices in $T$		
			$\Delta_d$	$\Delta_w$	$\Delta_m$	$\Delta_d$	$\Delta_w$	$\Delta_m$	$\Delta_d$	$\Delta_w$	$\Delta_m$	$\Delta_d$	$\Delta_w$	$\Delta_m$
Btc2011	1,987,113	3,909,286	10,127	55,290	212,921	11,748	82,397	362,380	1.33	1.59	1.82	1.31	1.65	1.89
Btc2012	8,577,776	18,389,841	36,651	220,058	992,282	52,554	369,522	1,804,755	1.63	1.89	2.17	1.57	1.86	2.10
Btc2013	19,658,304	43,570,830	83,924	502,205	2,072,286	127,588	900,325	3,995,375	1.73	2.00	2.19	1.70	1.99	2.16
Eth2016	670,559	13,654,676	19,720	92,361	368,071	43,209	311,628	1,394,052	5.69	6.25	7.15	3.63	5.67	4.93
Eth2021	58,274,378	461,781,254	600,576	3,275,312	11,740,881	1,326,215	9,536,231	41,863,219	1.82	2.21	1.90	2.75	1.64	2.62
IBM	2,116,168	179,702,229	38,721,761			216,307,822			147.67			105.57		

TABLE II: FCT vs. DIN-TF vs. DIN-RTF on the whole network ("Trans." represents the time taken for network transformation, and "% of Trans." indicates the percentage of network transformation time relative to the total query time of DIN-RTF).

Datasets	Query Efficiency without / with Transformation					Performance of Max. Flow Value			Distance	Peak Memory (MB)			
	FCT (ms)	DIN-TF (ms)	DIN-RTF			FCT	DIN-TF	DIN-RTF		FCT	DIN-TF	DIN-RTF	
			Trans. (ms)	Total Query Time (ms)	% of Trans.								
Btc2011	6	0.9	1.3	174	0.74	0.0017	0.060	<b>2.99</b>	165	271	89	89	
Btc2012	6,134	13	28	4,472	0.63	0.0002	0.021	<b>1.59</b>	43	1,259	431	432	
Btc2013	7,952	47	103	16,780	0.62	0.0005	0.023	<b>0.70</b>	23	2,935	926	948	
Eth2016	6	4	15	1,231	1.24	7.34	65,659	<b>214.66</b>	5,074	316	237	240	
Eth2021	970	941	941	55,371	1.70	0.04	0.422	<b>1.46</b>	108	19,359	6,686	6,695	
IBM	52,680	12	39	401	8.83	14K	98K	<b>98K</b>	5	3,201	3,046	3,047	

**Queries.** For each selected timespan, we randomly generate 50 pairs of sets  $S$  and  $T$ , as queries, which satisfy the following conditions: 1)  $\forall s_i \in S, \deg^{\text{out}}(s_i) \geq 1$  and  $\forall t_i \in T, \deg^{\text{in}}(t_i) \geq 1$ , and 2)  $|S| = |T| = \frac{n}{2}$ , where  $n$  is the parameter called the size of the queries. For the IBM synthetic transaction dataset, queries are generated on the entire graph, following the same query-generation procedure. Table I summarizes some characteristics of the datasets and queries. When investigating efficiency, we may discuss the term maximum flow as it helps to analyze the runtime, and it is different from the densest flow by a factor of  $|S'| + |T'|$ .

**Parameters.** For the query  $Q = (S, T, k)$  of  $\mathcal{T}$ -STDF, the number of sources and sinks, denoted as  $n = |S| + |T|$ , affects scalability, while  $k$  influences the detection of the flow density. To demonstrate the efficiency with respect to the query size, we vary  $n$  to be 16, 32, and 64. To illustrate how  $k$  affects the flow density, we vary  $k$  among 6, 8, and 10. The default values for  $k$  and  $n$  are set to 6 and 32, respectively.

**Algorithms.** We investigate two major performance factors of Conan, each investigation includes the respective related competitors. We first compare the efficiency and effectiveness of our graph transformation technique (Section IV). The competitors are listed as follows:

- 1) **FCT.** The network transformation of [41] represents the most recent work closely related to temporal flow detection. For a fair comparison, we adopt their default settings, including all optimization features.
- 2) **DIN-TF & DIN-RTF.** We implement the Dinic's algorithm in [18] on the TFN and the RTFN, respectively.

We use 1,000 random queries with a single source  $s$  and a single sink  $t$ . We set a time threshold of 1,000 seconds. We denote the queries that exceed this threshold as "Did Not Finish" (DNF). To investigate into the efficiency of the query evaluation of Conan, we compare four variants as follows:

- 1) **DC.** This baseline constitutes the dense flow detection pipeline at Grab by enumerating all combinations of the subsets of  $S$  and  $T$ . We enhance this enumeration with the query decomposition and the densest flow merge techniques. Note that DC returns the exact answers for STDF queries.
- 2) **PEEL.** Our flow peeling algorithm (Algorithm 2).

3) **PEEL\*.** PEEL with the pruning (Algorithm 3).

4) **PEEL-DC.** We combine PEEL and DC (Section VI-C).

5) **PEEL-DC\*.** PEEL-DC with the pruning (Section VI-B).

#### B. Effectiveness of Network Transformation (Stage 1)

**Impact on Query Time.** For a TFN, we obtain its corresponding RTFN by using the network transformation (Section IV). Notably, the network transformation time for RTFN remains under 1 second for all datasets. Further, Table II reports the average runtimes of DIN-TF and DIN-RTF for 1,000 random queries on respective datasets, each with a single source  $s$  and a single sink  $t$ . As Table II illustrates, the network transformation time for these queries constitutes less than 1.7% of the total query duration. Additionally, our experiments corroborate that the time required for network transformation is *linear* to the network size.

**Impact on Maximum Flow Value.** In Table II, we also present the results of the maximum flow values computed by [18] on TFN and RTFN, respectively. On Btc2011 (resp. Btc2012, Btc2013, Eth2016 and Eth2021), the maximum flow value of DIN-TF is only 2.0% (resp. 1.3% 3.3% 30.6% and 28.8%) as much as that of DIN-RTF. This verified that our network processing techniques successfully addressed the problems caused by temporal flow constraint in TFN and enabled determining much larger flow values. The implementation of FCT [41] consists of two primary steps: path enumeration and flow computation. Compared with both DIN-TF and DIN-RTF, FCT consistently yields even smaller flow values. This is primarily due to its hop-bounded path enumeration strategy: FCT enumerates only temporal paths up to a fixed length, which is often shorter than the actual flow distances observed in our queries (with average flow distance exceeding 20 on both BTC and ETH datasets).

**FCT vs. DIN-TF vs. DIN-RTF.** During our evaluations, we found that increasing the default path length significantly hindered FCT's ability to complete path enumeration on most of our datasets. Consequently, we adhered to FCT's default settings with all optimizations. Next, we highlight the results we obtained: DIN-TF detected up to 105 times and at least 7 times more flow than FCT. Moreover, DIN-RTF identified up to 7,945 times more flow than FCT. These discrepancies are caused by FCT's path enumeration strategy, which only

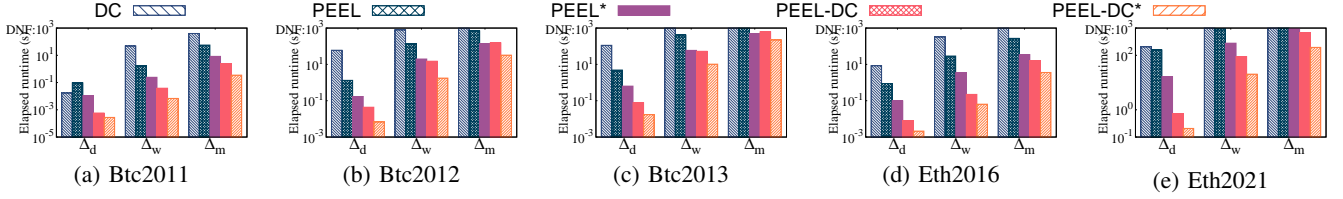


Fig. 10: Elapsed runtime of algorithms on the five real-world datasets under the default settings

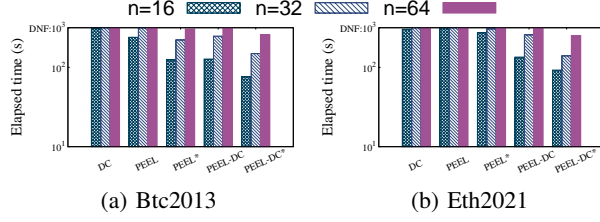


Fig. 11: Elapsed time by varying  $n$  (with  $k = 6$ )

considers paths within a certain length, potentially leading to the loss of flow. Notably, DIN-RTF consistently returned significantly larger temporal flows. In terms of efficiency, DIN-TF always outperformed FCT on all datasets, particularly on BTC2012 where it required as little as 0.21% of FCT's time. *In addition, DIN-TF and DIN-RTF also exhibit substantially lower peak memory usage than FCT, since they avoid explicit path materialization and operate on compact transformed networks (Table II).*

### C. Efficiency of Query Evaluation (Stage 2)

**Overall Efficiency (Figure 10).** We show the efficiency of the benchmarked techniques in various datasets using the default settings. It was found that PEEL-DC\* was the most efficient in all datasets. Specifically, a) on average, PEEL-DC\* was 4.9 (resp. 6.5, 4.1, 3.9 and 3.8) times more efficient than PEEL-DC in Btc2011 (resp. Btc2012, Btc2013, Eth2016, and Eth2021) due to the pruning technique, which avoids an enumeration during each peeling step. Additionally, b) when compared to PEEL\*, PEEL-DC\* had a speedup of 33 (resp. 14, 15, 37 and 33) times on Btc2011 (resp. Btc2012, Btc2013, Eth2016, and Eth2021) on average. The divide-and-conquer approach reduces the number of peeling iterations due to smaller query sets. Furthermore, c) PEEL-DC\* had a speedup of 253 (resp. 97, 110, 313 and 270) times when compared to PEEL on Btc2011 (resp. Btc2012, Btc2013, Eth2016 and Eth2021) on average. This is because PEEL requires  $n^2$  ( $n = 32$  in our default setting) times the maximum flow computation, which is still time-consuming. Lastly, d) it is not surprising that PEEL-DC\* was 2,745 (resp. 3,087, 2,205, 3,111 and 349) times more efficient than DC in Btc2011 (resp. Btc2012, Btc2013, Eth2016, and Eth2021) on average since DC enumerates each combination and computes the corresponding maximum flow as discussed in Section VI. The improvement is more obvious in smaller datasets since  $S$  and  $T$  has a higher chance of dividing into smaller subsets that the divide-and-conquer approach is more efficient.

**Improvement of DC.** We further investigate the impact of the divide-and-conquer technique. Our experiments, as shown in Figure 10, demonstrate that PEEL-DC (Section VI-C) is up to 219 (resp. 129 and 23) times faster than PEEL w.r.t.

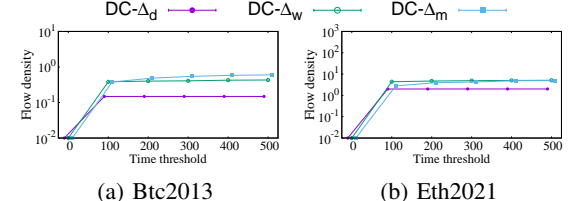


Fig. 12: Flow density of DC for queries of different timespans (denoted by the subscript) under different time thresholds

$\Delta_d$  (resp.  $\Delta_w$  and  $\Delta_m$ ). On average, PEEL-DC is 117 (resp. 40 and 10) times faster than PEEL w.r.t.  $\Delta_d$  (resp.  $\Delta_w$  and  $\Delta_m$ ). Additionally, we compare the elapsed time of PEEL\* and PEEL-DC\*. The findings demonstrate that PEEL-DC achieves speed improvements of up to 81 times (and 55 times and 24 times) compared to PEEL for the different time spans  $\Delta_d$ ,  $\Delta_w$ , and  $\Delta_m$ , respectively. On average, PEEL-DC\* is 46 (resp. 24 and 9) times faster than PEEL\* w.r.t.  $\Delta_d$  (resp.  $\Delta_w$  and  $\Delta_m$ ). This verifies that it is efficient to divide sets  $S$  and  $T$  into smaller subsets  $S_i$  and  $T_i$ , resulting in significantly fewer combinations of  $S_i$  and  $T_i$  in query evaluation.

**Improvement of Pruning.** We next evaluate the impact of the pruning technique (Line 11 of Algorithm 3). As shown in Figure 10, PEEL\* is up to 17 (resp. 278 and 934) times faster than PEEL w.r.t.  $\Delta_d$  (resp.  $\Delta_w$  and  $\Delta_m$ ). On average, PEEL\* is 4 (resp. 72 and 321) times faster than PEEL w.r.t.  $\Delta_d$  (resp.  $\Delta_w$  and  $\Delta_m$ ). We also compare the performance improvement of the pruning technique in PEEL-DC\*. PEEL-DC\* is up to 6 (resp. 9 and 7) times faster than PEEL-DC w.r.t.  $\Delta_d$  (resp.  $\Delta_w$  and  $\Delta_m$ ). On average, PEEL-DC\* is 4.0 (resp. 5.4 and 4.4) times faster than PEEL-DC w.r.t.  $\Delta_d$  (resp.  $\Delta_w$  and  $\Delta_m$ ). The reason for such an improvement is that the lower bounds of the peeling flow prune some unnecessary enumerations.

**Impact of the Timespans.** We evaluate the impact of the timespans by varying the length of the timespans on the performance of the compared algorithms. a) Not surprisingly, as the length of the timespans increases, all algorithms take longer to finish. This is consistent with the time complexity of the maximum flow  $O(M)$ , where  $M = |V|^2|E|$ , as  $M$  is the factor of the complexities of the algorithms for STDF. b) It is important to note that DC, PEEL and PEEL\* fail to return the densest flow over long timespans, whereas PEEL-DC and PEEL-DC\* can detect the densest flow over all timespans. As indicated in Section VI, the main bottleneck of STDF is the time to calculate the maximum flow, which can be well reduced by PEEL-DC and PEEL-DC\*.

**Impact of  $n$ .** The time complexity of the compared algorithms using PEEL is relevant to the parameter  $n$ , i.e., the size of the query vertex sets. In Figure 11, we present the runtimes of the compared algorithms on two larger datasets, Btc2013 and

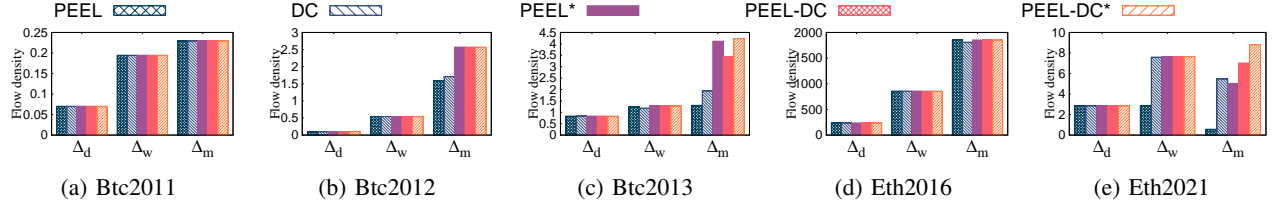


Fig. 13: Flow density of algorithms on the five real-world datasets under default settings

TABLE III: Peak memory (MB) of algorithms on five real-world datasets under the default settings. Numbers in parentheses are normalized to DC (lower is better).

Dataset	DC	PEEL	PEEL*	PEEL-DC	PEEL-DC*
Btc2011	1.129 (100.00%)	11 (0.97%)	11 (0.97%)	6 (0.53%)	6 (0.53%)
Btc2012	1.176 (100.00%)	65 (5.53%)	65 (5.53%)	25 (2.13%)	25 (2.13%)
Btc2013	1.160 (100.00%)	115 (9.91%)	115 (9.91%)	47 (4.05%)	47 (4.05%)
Eth2016	1.116 (100.00%)	42 (3.76%)	42 (3.76%)	15 (1.34%)	15 (1.34%)
Eth2021	1.641 (100.00%)	1,200 (73.12%)	1,200 (73.12%)	478 (29.13%)	478 (29.13%)
IBM	27,050 (100.00%)	27,048 (99.99%)	26,929 (99.55%)	8,532 (31.54%)	8,532 (31.54%)

Eth2021, for different values of  $n$ . As expected, the runtimes of the compared algorithms increase as  $n$  increases.

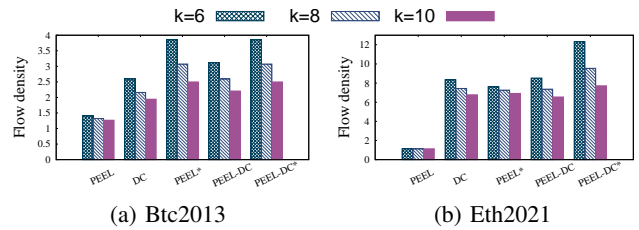
**Peak Memory Usage.** To further assess space efficiency, we profiled the peak memory of each method on the same platform and query set. Table III reports the peak memory consumption in megabytes (MB) on all datasets, with values in parentheses normalized to DC. Overall, the reduction in memory footprint mainly comes from *the search space reduction and avoiding maintaining a large number of max-flow instances simultaneously*, rather than from pruning itself. Compared to DC, the PEEL-based variants use substantially less memory, because PEEL limits the amount of intermediate max-flow state that needs to be maintained. As a result, PEEL\* (resp. PEEL-DC\*) consumes only around 32.14% (resp. 11.46%) of DC’s peak memory on average.

#### D. Effectiveness of Conan

**Flow Density of DC.** In Figure 12, we present the average maximum flow densities of DC for 1,000 random queries under different thresholds of elapsed time for the three types of timespans in Btc2013 and Eth2021 datasets. In a nutshell, the *denser* the detected flow, the *more effective* the method. The computed maximum flow density increases rapidly in the first 100 seconds. However, after 500 seconds, the flow density value increases slowly in all scenarios. Based on these observations, we set the elapsed time threshold to 1,000 seconds and DC is configured to return the densest flow found within this time threshold.

**Approximation Quality.** We further compare the solution quality of our peeling-based methods against the exact baseline DC on instances where DC is able to complete. The results show that all peeling variants produce solutions extremely close to the optimum. Specifically, PEEL and PEEL\* differ from DC by only 0.03% on average, while the hybrid variants PEEL-DC and PEEL-DC\* further reduce the average difference to 0.01%. These results indicate that, in practice, the proposed peeling-based algorithms incur negligible loss in solution quality while achieving performance improvements.

**Overall Effectiveness (Figure 13).** We present the effectiveness of the five techniques in terms of flow density. a) In most cases, PEEL-DC\* found the densest flow among the five techniques. In our experiments, PEEL-DC\* is capable of

Fig. 14: Flow density of algorithms by varying  $k$  (with  $n = 32$ )

returning the results *before* the threshold. On average, PEEL-DC\* detects 1.15 (resp. 1.26, 1.03, and 1.03) times denser flow than DC (resp. PEEL, PEEL\* and PEEL-DC). b) Compared to the exact algorithm DC, we observe that although DC is able to return answers for all queries on smaller datasets, such as Btc2011, PEEL-DC\* is still very competitive. We denote the relative error by  $\epsilon = \frac{g - \hat{g}}{g}$  to measure the densest quality, where  $\hat{g}$  and  $g$  are the flow densities of DC and PEEL-DC\*, respectively. Our experiment shows that PEEL-DC\* introduces an error of only 0.2%, w.r.t.  $\Delta_d$ . It is noteworthy that, despite DC’s capability to return exact answers, DC cannot finish all possible subset combinations, resulting in a lower flow density at the termination due to the time threshold.

**Impact of  $k$ .** In Figure 14, we examine the impact of the parameter  $k$  on the flow densities. By varying  $k$  to 6, 8, and 10, we observe the following: a) PEEL-DC\* consistently outperforms the other algorithms in finding the densest flows. b) As  $k$  increases, the flow density decreases.

## VIII. INDUSTRIAL APPLICATION

### A. Case Study 1: Application of Conan within Grab

**Dataset Description.** To validate the practicality of Conan, we tested its efficiency and effectiveness on an industry dataset, GFG, provided by Grab. GFG comprises a transaction flow network with  $|V| = 3.38M$  nodes and  $|E| = 28.64M$  edges, where each node represents entities such as users, merchants, digital wallets, or card numbers. Each edge represents transactions or transfer records between these nodes (all data have been normalized to large random values for business privacy).

**Flow Density as a Fraud Indicator.** We examined the flow densities of different fraudulent and benign groups, using ground truth provided by Grab. For each group size, we collected 100 samples of fraudulent groups. If a node among the suspects had larger outgoing funds than incoming funds, we allocated it to  $S$ ; if the incoming flow was greater, it was assigned to  $T$ . As illustrated in Figure 15, fraudulent groups tend to exhibit higher flow density compared to benign ones, underscoring flow density as a strong indicator of fraudulent activity. The figure also reveals that smaller groups have higher flow density, highlighting the necessity of controlling group

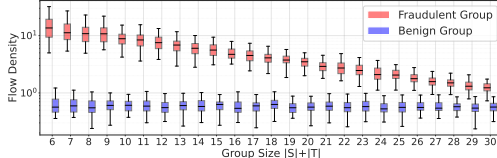


Fig. 15: Distribution of Flow Density by Group Size

size in queries. Without a minimum size threshold  $k$ , queries might only return small groups, potentially overlooking larger fraud networks. By enforcing the  $k$  parameter, STDF captures extensive fraud networks, increasing the likelihood of identifying a broader range of fraudulent actors.

**Query Formulation.** We used **Spade** [37] to identify suspects. **Spade** supports three density metrics: *dense subgraphs* (DG [7]), *dense weighted subgraphs* (DW [26]), and *Fraudar-based density* (FD [30]). We divided the detected suspects into query sets  $S$  and  $T$  for each mode. If a node had larger outgoing funds than incoming funds among the suspects, we allocated it to  $S$ ; if the incoming flow was greater, it was assigned to  $T$ . We then utilized  $S$  and  $T$  as queries, setting  $k$  to 20% of  $|S|+|T|$ , i.e.,  $k = 470$ .

**Impact of Temporal Dependency.** We compared the detection results with and without incorporating temporal dependencies. We observed that neglecting temporal dependencies led to detecting only 22.7% of the flow volume. Specifically, precision merely increased from 64.93% to 82.39%, a less substantial improvement compared to cases considering temporal dependencies. These results underscore the critical role of temporal context in improving the accuracy of fraud detection, emphasizing the need for methodologies that account for the timing of transactions.

**Efficiency and Effectiveness.** Since DC could not finish within an hour, we limited our comparison to four algorithms of **Conan** and **Spade**. The results are illustrated in Figure 16. PEEL-DC\* took only 1.04%, 0.43%, and 0.14% of the time that **Spade** takes, respectively, yet detected 3.51×, 8.41×, and 3.70× denser money flows under DG, DW, and FD modes. This significantly reduces the time needed for manual screening and verification at Grab. It is worth noting that the detection pipeline in Grab, DC, could not complete the STDF queries within 24 hours, whereas PEEL-DC\* typically completed the STDF queries in about one second.

**Detection of Credit Card Fraud.** Compared to the ground truth provided by Grab, only 64.9% of the cases reported by **Spade** are fraudsters or fraudulent cards. The precision is enhanced from 64.9% to 95.8%, and the flow density is increased from 0.46 to 0.80 (after normalizing the amounts to random values). This improvement is attributed to the flow peeling, which excludes users with lower participation.

#### B. Case Study 2: Application of Conan within NFT

We employed **Conan** to examine instances of wash trading fraud in the NFT network. In this study, we leveraged known wash trading fraud identified in NFT communities [1] as ground truth. The query formulation is identical to that in Section VIII-A. Previous research [37], [26], [30] has shown limited success in accurately identifying suspicious addresses; only 55.61% of the suspects ( $S$  and  $T$  detected by **Spade**)

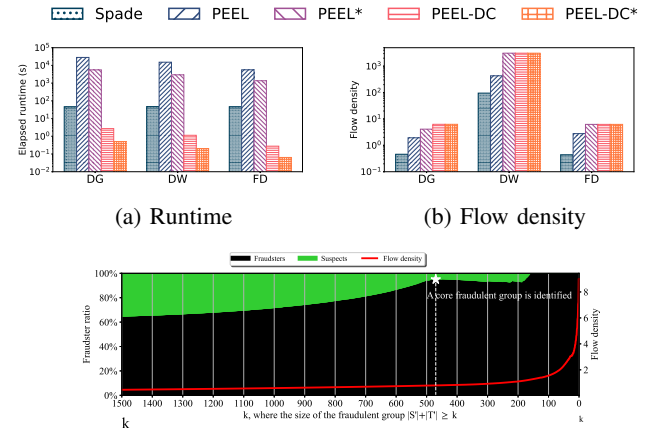


Fig. 16: Case study on Grab transaction networks

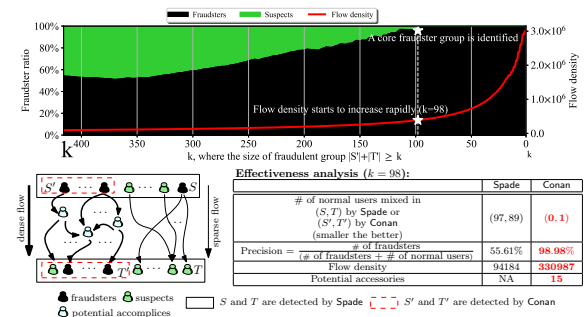


Fig. 17: Case Study on NFT Networks

are true fraudsters. **Conan** detects the densest flow from  $S$  to  $T$  and obtains subsets  $S'$  and  $T'$ . We show the impact of the parameter  $k$  at the top of Figure 17. If  $k$  is smaller, more vertices are peeled, leaving only the core fraudsters and resulting in denser flows, as indicated by the red line. When  $k = 98$ , the flow density increases rapidly and a core fraudulent group,  $S'$  and  $T'$ , is identified. The flow density increases from 94,184 to 330,987, and the precision increases from 55.61% to 98.98%. We investigate the vertices in the flow between  $S'$  and  $T'$  and spot 15 fraudsters not identified by **Spade**.

**Summary.** Our case studies demonstrate the effectiveness of **Conan** in (1) identifying meaningful fraudulent communities in real-life transaction flow networks, (2) tracking money transfers among fraudsters, and (3) revealing more potential accomplices. By setting  $k$  between  $0.2 \times (|S|+|T|)$  and  $0.3 \times (|S|+|T|)$ , **Conan** returns a core fraudulent group.

## IX. RELATED WORK

**Query Processing on Temporal Graphs.** Recently, there has been a growing interest in query processing on temporal graphs from both the industry and research communities (e.g., [41], [65], [66], [72], [71]). The most relevant work to this paper is Kosyfaki et al. [41]. They defined two flow transfer models on temporal networks but only focused on the temporal flow problem between a single source  $s$  and a single sink  $t$ . The authors solution for maximum temporal flow applies to graphs with a maximum of 10K transactions, owing to the quadratic time complexity. In contrast, **Conan** aims to find the densest flow of two given sets  $S$  and  $T$ .

**Dense Subgraph Detection.** Current research in detecting fraudulent activities has predominantly focused on dense sub-

graph discovery techniques, as detailed in studies like [37], [30], [54], [26], [45], [34], [11], [73], [9], [44], [49], [35], [36]. However, these methods often fail to account for the complexities of layering transfer schemes, crucial in fraud detection. Though the approach in [43] emphasizes detecting dense flows, it is confined to strictly  $k$ -partite data and lacks adaptability to more intricate network structures, as indicated by [59]. Furthermore, existing studies on dense flow detection tend to overlook the temporal dependencies in transaction networks, which can significantly impact detection effectiveness. In addition to these algorithmic efforts, several labeled benchmarks have been released to support fraud and phishing detection in transaction graphs. Notably, the Ethereum phishing-label transaction dataset released by InPlusLab has been used for graph-based phishing and fraud detection in Ethereum networks [10]. **Conan** sets itself apart as the first framework to focus on layering transfer schemes densest flow queries, incorporating temporal dependency for enhanced precision in fraud detection applications.

**Maximum Flow.** Over the past few decades, many solutions have been proposed to solve the maximum-flow problem. Ford et al. [21] introduced the first feasible-flow algorithm by iteratively finding the augmenting paths. Dinic [18] built a layered graph with a breadth-first search on the residual graph to return the maximum flow in a layered graph in  $O(|V|^2|E|)$ . Goldberg et al. [24] proposed the push-relabel method with a time complexity of  $O(|V|^3)$ . Hochbaum [28] used a normalized tree to organize all unsaturated arcs, then the process of finding augmenting paths can be accelerated to  $O(|V||E|\log|V|)$  by incorporating the dynamic tree. Hochstein et al. [29] optimized the push-relabel algorithm and calculated the maximum flow of a network with  $k$  crossings in  $O(k^3|V|\log|V|)$  time. Chen et al. [8] introduced an algorithm capable of nearly linearly addressing maximum and minimum-cost flow problems by constructing flows through a sequence of approximate undirected minimum-ratio cycles. While this method represents a significant theoretical advancement, its practical implementation remains an open challenge. **Conan** stands out, differing in two significant ways: (a) **Conan** pioneers the incorporation of a densest flow query; and (b) **Conan** returns the maximum temporal flow in transaction networks with temporal dependencies. Hence, **Conan** operates orthogonally to the individual maximum flow algorithms.

**Temporal Flow.** There are a few studies on flows under temporal constraints. Horst et al. [27] investigate the effects of time-varying capacities on maximum flow in temporal graphs. Akrida et al. [4] treat flow networks as ephemeral entities, with each edge available only during certain times, and analyze maximum flow within specific time intervals. The concept of earliest arrival flow, explored in studies [50], [22], [63], [55], focuses on determining the earliest time for a flow to travel from  $s$  to  $t$ . **Conan** is the first framework to concentrate on flow density with a temporal flow dependency.

## X. CONCLUSIONS

Grab practices advanced fraud detection techniques to combat sophisticated fraudulent activities in its transaction

networks. However, existing methods face challenges in scalability and effectiveness when dealing with large-scale data and complex fraud patterns. To address these issues, we propose a novel query called STDF, specifically designed to detect fraud in transaction networks. We introduce an efficient solution, **Conan**, to solve STDF. **Conan** incorporates a network transformation technique that ensures the correct maximum temporal flow is returned, allowing seamless integration with existing maximum flow algorithms. Our experiments demonstrate that **Conan** is efficient and effective, with query evaluations up to three orders of magnitude faster than baseline algorithms. Deployment of **Conan** in operational environments has significantly improved fraud detection accuracy and processing speed, leading to reduced financial losses for Grab.

## REFERENCES

- [1] DUNE. [https://dune.com/qboy29/looks\\_rare\\_wash\\_trades](https://dune.com/qboy29/looks_rare_wash_trades).
- [2] Efficient densest flow queries in transaction flow networks. [https://anonymous.4open.science/r/CONAN-IMPL-34CE/CONAN\\_TKDE.pdf](https://anonymous.4open.science/r/CONAN-IMPL-34CE/CONAN_TKDE.pdf), 2024.
- [3] R. K. Ahuja, T. L. Magnanti, and J. B. Orlin. *Network flows: theory, algorithms, and applications*. Prentice hall, 1993.
- [4] E. C. Akrida, J. Czyzowicz, L. Gąsieniec, Ł. Kuszner, and P. G. Spirakis. Temporal flows in temporal networks. *Journal of Computer and System Sciences*, pages 46–60, 2019.
- [5] E. Altman, J. Blanuša, L. Von Niederhäusern, B. Egressy, A. Anghel, and K. Atasu. Realistic synthetic financial transactions for anti-money laundering models. *Advances in Neural Information Processing Systems*, 36:29851–29874, 2023.
- [6] S. Cao, X. Yang, C. Chen, J. Zhou, X. Li, and Y. Qi. Titant: online real-time transaction fraud detection in ant financial. In *Proceedings of the VLDB Endowment*, volume 12, pages 2082–2093, 2019.
- [7] M. Charikar. Greedy approximation algorithms for finding dense components in a graph. In *International Workshop on Approximation Algorithms for Combinatorial Optimization*, pages 84–95. Springer, 2000.
- [8] L. Chen, R. Kyng, Y. P. Liu, R. Peng, M. P. Gutenberg, and S. Sachdeva. Maximum flow and minimum-cost flow in almost-linear time. In *2022 IEEE 63rd Annual Symposium on Foundations of Computer Science (FOCS)*, pages 612–623. IEEE, 2022.
- [9] L. Chen, C. Liu, R. Zhou, K. Liao, J. Xu, and J. Li. Densest multipartite subgraph search in heterogeneous information networks. *Proceedings of the VLDB Endowment*, 17(4):699–711, 2023.
- [10] L. Chen, J. Peng, Y. Liu, J. Li, F. Xie, and Z. Zheng. XBLOCK Blockchain Datasets: InPlusLab ethereum phishing detection datasets. <http://xblock.pro/ethereum/>, 2019.
- [11] Y. Chen, J. Jiang, S. Sun, B. He, and M. Chen. Rush: Real-time burst subgraph detection in dynamic graphs. *Proceedings of the VLDB Endowment*, 17(11):3657–3665, 2024.
- [12] J. Cheng, S. Huang, H. Wu, and A. Fu. Tf-label: a topological-folding labeling scheme for reachability querying in a large graph. In *Proceedings of the ACM SIGMOD International Conference on Management of Data*, pages 193–204, 2013.
- [13] B. V. Cherkassky and A. V. Goldberg. On implementing the push-relabel method for the maximum flow problem. *Algorithmica*, pages 390–410, 1997.
- [14] A. F. Colladon and E. Remondi. Using social network analysis to prevent money laundering. *Expert Systems with Applications*, pages 49–58, 2017.
- [15] L. W. Cong, X. Li, K. Tang, and Y. Yang. Crypto wash trading. Technical report, National Bureau of Economic Research, 2022.
- [16] L. Delamaire, H. Abdou, and J. Pointon. Credit card fraud and detection techniques: a review. *Banks and Bank systems*, 4(2):57–68, 2009.
- [17] M. Di Gennaro, F. Panebianco, M. Pianta, S. Zanero, and M. Carminati. Amatriciana: Exploiting temporal gnns for robust and efficient money laundering detection. In *2024 IEEE International Conference on Data Mining Workshops (ICDMW)*, pages 254–261. IEEE, 2024.
- [18] E. A. Dinic. Algorithm for solution of a problem of maximum flow in networks with power estimation. *In Soviet Math. Doklady*, volume 11, pages 1277–1280, 1970.

[19] Y. Dou, Z. Liu, L. Sun, Y. Deng, H. Peng, and P. S. Yu. Enhancing graph neural network-based fraud detectors against camouflaged fraudsters. In Proceedings of the 29th ACM International Conference on Information & Knowledge Management, pages 315–324, 2020.

[20] U. Feige, M. Seltser, et al. On the densest k-subgraph problem. Citeseer, 1997.

[21] L. R. Ford and D. R. Fulkerson. Maximal flow through a network. Canadian journal of Mathematics, pages 399–404, 1956.

[22] D. Gale. Transient flows in networks. Michigan Mathematical Journal, pages 59–63, 1959.

[23] B. Gao, H. Wang, P. Xia, S. Wu, Y. Zhou, X. Luo, and G. Tyson. Tracking counterfeit cryptocurrency end-to-end. Proceedings of the ACM on Measurement and Analysis of Computing Systems, 4(3):1–28, 2020.

[24] A. V. Goldberg and R. E. Tarjan. A new approach to the maximum-flow problem. Journal of the ACM (JACM), pages 921–940, 1988.

[25] O. M. Granados and A. Vargas. The geometry of suspicious money laundering activities in financial networks. EPJ Data Science, 11(1):6, 2022.

[26] N. V. Gudapati, E. Malaguti, and M. Monaci. In search of dense subgraphs: How good is greedy peeling? Networks, 77(4):572–586, 2021.

[27] H. W. Hamacher and S. A. Tjandra. Earliest arrival flows with time-dependent data. 2003.

[28] D. S. Hochbaum. The pseudoflow algorithm: A new algorithm for the maximum-flow problem. Operations research, pages 992–1009, 2008.

[29] J. M. Hochstein and K. Weihe. Maximum st-flow with  $k$  crossings in  $O(k \sqrt{n} \log n)$  time. In Proceedings of the eighteenth annual ACM-SIAM symposium on Discrete algorithms, pages 843–847, 2007.

[30] B. Hooi, H. A. Song, A. Beutel, N. Shah, K. Shin, and C. Faloutsos. Fraudar: Bounding graph fraud in the face of camouflage. In Proceedings of the 22nd ACM SIGKDD international conference on knowledge discovery and data mining, pages 895–904, 2016.

[31] Y. Hu, S. Seneviratne, K. Thilakarathna, K. Fukuda, and A. Seneviratne. Characterizing and detecting money laundering activities on the bitcoin network. arXiv preprint arXiv:1912.12060, 2019.

[32] X. Huang, Y. Yin, S. Lim, G. Wang, B. Hu, J. Varadarajan, S. Zheng, A. Bulusu, and R. Zimmermann. Grab-posisi: An extensive real-life gps trajectory dataset in southeast asia. In Proceedings of the 3rd ACM SIGSPATIAL international workshop on prediction of human mobility, pages 1–10, 2019.

[33] Y. Huang et al. Graph-based feature learning for anti-money laundering in cross-border transaction networks. Journal of Advanced Computing Systems, 4(7):39–49, 2024.

[34] J. Jiang, Y. Chen, B. He, M. Chen, and J. Chen. Spade+: A generic real-time fraud detection framework on dynamic graphs. IEEE Transactions on Knowledge and Data Engineering, 2024.

[35] J. Jiang, S. Yao, Y. Chen, B. He, Y. Niu, Y. Li, S. Sun, and Y. Liu. Community detection in heterogeneous information networks without materialization. In ACM SIGMOD/PODS International Conference on Management of Data., 2025.

[36] J. Jiang, S. Yao, Y. Li, Q. Wang, B. He, and M. Chen. Dupin: A parallel framework for densest subgraph discovery in fraud detection on massive graphs. In ACM SIGMOD/PODS International Conference on Management of Data., 2025.

[37] J. Jiaxin, L. Yuan, H. Bingsheng, H. Bryan, C. Jia, and J. K. Z. Kang. A real-time fraud detection framework on evolving graphs. PVLDB, 2023.

[38] R. Jin, N. Ruan, S. Dey, and J. Y. Xu. Scarab: scaling reachability computation on large graphs. In Proceedings of the ACM SIGMOD International Conference on Management of Data, pages 169–180, 2012.

[39] R. Jin, N. Ruan, Y. Xiang, and H. Wang. Path-tree: An efficient reachability indexing scheme for large directed graphs. ACM Trans. Database Syst., pages 7:1–7:44, 2011.

[40] D. Kondor and M. Pósfai. Principal component analysis of the cryptocurrency market. PloS one, 13(11):e0208535, 2018.

[41] C. Kosyfaki, N. Mamoulis, E. Pitoura, and P. Tsaparas. Flow computation in temporal interaction networks. In 2021 IEEE 37th International Conference on Data Engineering (ICDE), pages 660–671. IEEE, 2021.

[42] D. V. Kute, B. Pradhan, N. Shukla, and A. Alamri. Deep learning and explainable artificial intelligence techniques applied for detecting money laundering—a critical review. IEEE access, 9:82300–82317, 2021.

[43] X. Li, S. Liu, Z. Li, X. Han, C. Shi, B. Hooi, H. Huang, and X. Cheng. Flowscope: Spotting money laundering based on graphs. In Proceedings of the AAAI conference on artificial intelligence, volume 34, pages 4731–4738, 2020.

[44] L. Liang, Y. Zhou, and Y. Fang. Accelerated coordinate descent for directed densest subgraph discovery. In Proceedings of the ACM SIGKDD Conference on Knowledge Discovery and Data Mining (KDD), 2026.

[45] S. Liu, B. Hooi, and C. Faloutsos. Holoscope: Topology-and-spike aware fraud detection. In Proceedings of the 2017 ACM on Conference on Information and Knowledge Management, pages 1539–1548, 2017.

[46] B. Luo, J. Jiang, Y. Chen, J. Hou, C. J. Tey, Z. Qiu, B. He, S. Xiao, D. Ong, and W. H. Ang. Rich: Real-time identification of negative cycles for high-efficiency arbitrage. Proceedings of the VLDB Endowment, 18(11):4081–4089, 2025.

[47] U. P. Modepalli. Network analytics for identifying fraud rings and systemic risk. Journal of Information Systems Engineering and Management, 10(58s):616–624, 2025. Open Access.

[48] M. Möser, R. Böhme, and D. Breuker. An inquiry into money laundering tools in the bitcoin ecosystem. In 2013 APWG eCrime researchers summit, pages 1–14, 2013.

[49] Y. Niu, Y. Li, J. Jiang, and L. V. Lakshmanan. Sans: Efficient densest subgraph discovery over relational graphs without materialization. In The Web Conference, 2025.

[50] M. Schmidt and M. Skutella. Earliest arrival flows in networks with multiple sinks. Discrete Applied Mathematics, pages 320–327, 2014.

[51] S. Serneels. Detecting wash trading for nonfungible tokens. Finance Research Letters, 52:103374, 2023.

[52] S. Shadrooh and K. Nørvåg. Smotef: Smurf money laundering detection using temporal order and flow analysis. Applied Intelligence, 54(15):7461–7478, 2024.

[53] O. Shafiq. Bitcoin transactions data 2011-2013, 2019.

[54] K. Shin, B. Hooi, J. Kim, and C. Faloutsos. Densealert: Incremental dense-subtensor detection in tensor streams. In Proceedings of the 23rd ACM SIGKDD International Conference on Knowledge Discovery and Data Mining, pages 1057–1066, 2017.

[55] M. Skutella. An introduction to network flows over time. In Research trends in combinatorial optimization, pages 451–482. Springer, 2009.

[56] M. Song, Y. Liu, A. Shah, and S. Chava. Abnormal trading detection in the nft market. KDD, 2023.

[57] M. R. Soudijn. Removing excuses in money laundering. Trends in Organized Crime, 15(2-3):146–163, 2012.

[58] J. Su, Q. Zhu, H. Wei, and J. X. Yu. Reachability querying: can it be even faster? IEEE Transactions on Knowledge and Data Engineering, pages 683–697, 2016.

[59] H. Tariq and M. Hassani. Topology-agnostic detection of temporal money laundering flows in billion-scale transactions. arXiv preprint arXiv:2309.13662, 2023.

[60] A. Tošić, J. Vičič, and N. Hrovatin. Beyond the surface: advanced wash-trading detection in decentralized nft markets. Financial Innovation, 11(1):1–21, 2025.

[61] B. Villányi. Money laundering: History, regulations, and techniques. In Oxford Research Encyclopedia of Criminology and Criminal Justice, 2021.

[62] M. Weber, G. Domeniconi, J. Chen, D. K. I. Weidele, C. Bellei, T. Robinson, and C. E. Leiserson. Anti-money laundering in bitcoin: Experimenting with graph convolutional networks for financial forensics. CoRR, abs/1908.02591, 2019.

[63] W. L. Wilkinson. An algorithm for universal maximal dynamic flows in a network. Operations Research, pages 1602–1612, 1971.

[64] G. Wood. Ethereum: A secure decentralised generalised transaction ledger. Ethereum, 2014.

[65] H. Wu, J. Cheng, S. Huang, Y. Ke, Y. Lu, and Y. Xu. Path problems in temporal graphs. Proceedings of the VLDB Endowment, pages 721–732, 2014.

[66] H. Wu, Y. Huang, J. Cheng, J. Li, and Y. Ke. Reachability and time-based path queries in temporal graphs. In 2016 IEEE 32nd International Conference on Data Engineering (ICDE), pages 145–156, 2016.

[67] J. Wu, J. Liu, W. Chen, H. Huang, Z. Zheng, and Y. Zhang. Detecting mixing services via mining bitcoin transaction network with hybrid motifs. IEEE Transactions on Systems, Man, and Cybernetics: Systems, pages 1–13, 2021.

[68] J. Wu, Y. Yu, D. Lin, Z. Chen, and Z. Jiang. From shadows to light: Uncovering money laundering in ethereum transaction graphs. Available at SSRN 5076472.

[69] L. Xu, J. Jiang, B. Choi, J. Xu, and H. Bingsheng. Bursting flow query on large temporal flow networks. In ACM SIGMOD International Conference on Management of Data, 2025.

[70] C. Ye, Y. Li, B. He, Z. Li, and J. Sun. Gpu-accelerated graph label propagation for real-time fraud detection. In Proceedings of the 2021 International Conference on Management of Data, pages 2348–2356, 2021.

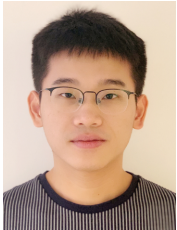
[71] Y. Yuan, X. Lian, G. Wang, Y. Ma, and Y. Wang. Constrained shortest path query in a large time-dependent graph. Proceedings of the VLDB Endowment, 12(10):1058–1070, 2019.

[72] T. Zhang, Y. Gao, L. Chen, W. Guo, S. Pu, B. Zheng, and C. S. Jensen. Efficient distributed reachability querying of massive temporal graphs. *The VLDB Journal*, 28(6):871–896, 2019.

[73] Y. Zhou, L. Liang, and Y. Fang. Efficient and scalable directed densest subgraph discovery. *Proceedings of the ACM on Management of Data*, 3(6):1–27, 2025.



**Bingsheng He** received the bachelor degree in computer science from Shanghai Jiao Tong University (1999-2003), and the PhD degree in computer science in Hong Kong University of Science and Technology (2003-2008). He is a professor in School of Computing, National University of Singapore. His research interests are high performance computing, distributed and parallel systems, and database systems. He is an ACM Distinguished member (class of 2020), and a fellow of IEEE (class of 2025).



**Jiaxin Jiang** is a senior research fellow in the School of Computing, National University of Singapore. He received his BEng degree in computer science and engineering from Shandong University in 2015 and PhD degree in computer science from Hong Kong Baptist University (HKBU) in 2020. His research interests include graph-structured databases, distributed graph computation and fraud detection.



**Yunxiang Zhao** received the BEng degree in computer science and engineering from East China Normal University in 2022. He is currently a PhD student in the Department of Computer Science, Hong Kong Baptist University. His research interests include graph data managements and time series analysis.



**Shixuan Sun** is a Tenure-Track Associate Professor at the Department of Computer Science and Engineering, Shanghai Jiao Tong University. He received his Ph.D. in Computer Sciences from the Department of Computer Science and Engineering, Hong Kong University of Science and Technology (HKUST) in 2020. Prior to that, he got his M.S and B.S. in Computer Sciences from the School of Software Engineering, Tongji University in 2014 and 2011 respectively. His research interests are in database systems, graph algorithms, and parallel computing. Current focus is on building high-performance graph data management systems.



**Lyu Xu** is currently a postdoctoral research fellow in the College of Computing and Data Science, Nanyang Technological University. He received his BEng degree in computer science and technology from Southeast University, MEng degree in computer science and technology from Sun Yat-sen University, and PhD degree in computer science from Hong Kong Baptist University (HKBU). His research interests include graph-structured databases and privacy preserving computation.



**Jia Chen** received his Bachelor degree in Automation from Tsinghua University (1999-2003) and the PhD degree in Computer Science from Hong Kong University of Science and Technology (2005-2009). He is currently Head of Data Science, Integrity at Grab. His research interests include efficient machine learning for large scale, high dimensional and real time data, and generative models for image and text.



**Byron Choi** is a Professor in the Department of Computer Science at the Hong Kong Baptist University. He received the bachelor of engineering degree in computer engineering from the Hong Kong University of Science and Technology (HKUST) in 1999 and the MSE and PhD degrees in computer and information science from the University of Pennsylvania in 2002 and 2006, respectively. His research interests include graph data management and time series analysis.

## APPENDIX

## A. NP-hardness

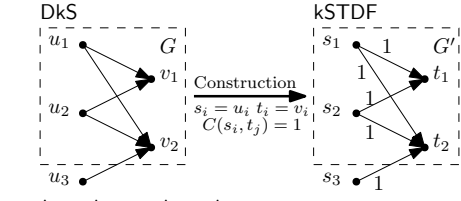


Fig. 18: Construction from DkS to STDF

**Lemma II.1.** *The decision problem of STDF is NP-complete.*

*Proof.* The STDF problem is provably NP-complete, demonstrated through a reduction from the decision problem of the densest subgraph with at least  $k$  vertices (DkS problem), as referred to in [20]. It's a known fact that the DkS problem is NP-complete even on bipartite graphs.

Given an instance of the DkS problem, denoted as  $G = (U \cup V, E)$ , we construct a corresponding instance of STDF as follows: We create a graph  $G' = (S \cup T, E', C)$  to serve as the input for STDF, wherein  $S = U$ ,  $T = V$ , the edge set  $(u, v) \in E'$  if and only if  $(u, v) \in E$ , and the capacity function  $C(u, v) = 1$  for all  $(u, v) \in E'$ . This construction, which is graphically represented in Figure 18, can be completed in polynomial time.

Let's define the induced subgraph of  $U' \cup V'$  in  $G$  as  $E(U', V')$ . It follows that  $|E(U', V')| = \text{MFLOW}(S', T')$ , where  $S' = U$  and  $T' = V$ . Given that  $|U'| + |V'| = |S'| + |T'|$ , the density of the induced subgraph by  $U' \cup V'$  can be expressed as  $\frac{|E(U', V')|}{|U'| + |V'|} = \frac{\text{MFLOW}(S', T')}{|S'| + |T'|} = g(S', T')$ . Therefore, if  $|S'| + |T'| \geq k$  and  $g(S', T')$  is maximized, then the density of the subgraph induced by  $U' = S'$  and  $V' = T'$  is also maximized.

Assuming that  $S'$  and  $T'$  can be determined in polynomial time, it then follows that  $U'$  and  $V'$  can also be found in polynomial time. However, this contradicts the NP-completeness of the DkS problem.  $\square$

## B. 3-Approximation

**Lemma VI.1.**  $\forall F \in [0, g(S, T)]$ ,  $\exists i \in [0, n]$ ,  $(S_i, T_i) = \text{FCore}(S, T)$ .

*Proof.* We prove the lemma in contradiction by assuming that  $\text{FCore}(S, T)$  does not exist, i.e.,  $\delta_i < F$ . We have the following contradiction.

$$\begin{aligned} \text{MFLOW}(S, T) &= \text{MFLOW}(S_n, T_n) = \text{MFLOW}(S_{n-1}, T_{n-1}) + \delta_n \\ &= \text{MFLOW}(S_{n-2}, T_{n-2}) + \delta_n + \delta_{n-1} = \dots \\ &= \text{MFLOW}(S_0, T_0) + \sum_{i=1}^n \delta_i = \sum_{i=1}^n \delta_i \\ &< nF \leq \frac{n \text{MFLOW}(S, T)}{n} = \text{MFLOW}(S, T) \end{aligned}$$

We can conclude that there exists  $\text{FCore}(S, T)$  for  $0 \leq F \leq g(S, T)$ .  $\square$

Given  $F \in [0, g(S, T)]$ , there might exist several  $\text{FCore}$ . In our following discussion, we only consider the  $\text{FCore}$  with the largest index  $i$  for  $S_i$  and  $T_i$ , i.e.,  $\delta_j < F$  for  $j \in (i, n]$ .

**Lemma VI.2.**  $\forall \alpha \in [0, 1]$  and  $F = \alpha g(S, T)$ ,  $\text{MFLOW}(S^F, T^F) \geq (1 - \alpha) \text{MFLOW}(S, T)$ , where  $(S^F, T^F) = \text{FCore}(S, T)$ .

*Proof.* We consider the maximum flow between  $S$  and  $T$ .

$$\begin{aligned} \text{MFLOW}(S, T) &= \sum_{j=1}^n \delta_j = \sum_{j=1}^i \delta_j + \sum_{j=i+1}^n \delta_j \\ &\leq \text{MFLOW}(S_i, T_i) + (n - i)F \\ &\leq \text{MFLOW}(S^F, T^F) + nF \end{aligned}$$

Therefore, we have the following conclusion.

$$\begin{aligned} \text{MFLOW}(S^F, T^F) &\geq \text{MFLOW}(S, T) - nF = \text{MFLOW}(S, T) - n\alpha g(S, T) \\ &= \text{MFLOW}(S, T) - \frac{n\alpha \text{MFLOW}(S, T)}{n} \\ &= (1 - \alpha) \text{MFLOW}(S, T) \end{aligned}$$

$\square$

**Theorem VI.3.** *Algorithm 2 is a 3-approximation algorithm.*

*Proof.* Consider the peeling sequence  $\{(S_n, T_n), \dots, (S_0, T_0)\}$ . Let  $(S', T')$  represent the exact solution to the STDF problem. For any integer  $k$ , there exists  $i \in [k, n]$  such that  $g(S_i, T_i) \geq \frac{g(S', T')}{3}$ .

Define  $\alpha = \frac{2}{3}$  and let  $F = \frac{2g(S', T')}{3}$ . According to Lemma VI.2, we have:

$$\text{MFLOW}(S'^F, T'^F) \geq \frac{\text{MFLOW}(S', T')}{3} \quad (6)$$

Since  $S'$  and  $T'$  are subsets of  $S$  and  $T$  respectively, we deduce that

$$\text{MFLOW}(S^F, T^F) \geq \frac{\text{MFLOW}(S', T')}{3} \quad (7)$$

By definition, the peeling flow of any vertex  $u$  is no less than  $F$ . Consequently, the total incoming flow to  $T^F$  equals the outgoing flow from  $S^F$ , leading to:

$$\begin{aligned} g(S^F, T^F) &\geq \frac{(|S^F| + |T^F|) \times F}{2 \times (|S^F| + |T^F|)} \\ &\geq \frac{g(S', T')}{3}. \end{aligned}$$

From Lemma VI.1, there exists some  $i$  such that  $(S_i, T_i) = \text{FCore}(S, T)$ , i.e.,  $S_i = S^F$  and  $T_i = T^F$ .

**Case 1:** If  $i \geq k$ , then  $(S_i, T_i)$  satisfies all requirements.

**Case 2:** If  $i < k$ , then  $(S_k, T_k)$  is a 3-approximation of the answer. Since  $(S', T')$  is the exact answer and due to the definition, we have

$$|S'| + |T'| \geq k \quad (8)$$

Then we have:

$$\begin{aligned}
 g(S_k, T_k) &= \frac{\text{MFLOW}(S_k, T_k)}{k} \\
 &\geq \frac{\text{MFLOW}(S_i, T_i)}{k} \quad \because S_i \subseteq S_k, T_i \subseteq T_k \\
 &\geq \frac{\text{MFLOW}(S', T')/3}{k} \quad \because \text{Equation 7} \\
 &\geq \frac{g(S', T')}{3} \quad \because \text{Equation 8}
 \end{aligned}$$

In either case, we establish that Algorithm 2 is a 3-approximation algorithm, concluding the proof.  $\square$

**Property 4.**  $\forall s \in S, t \in T$ , 1)  $\text{PF}(t, S \setminus \{s\}, T) \geq \text{PF}(t, S, T) - \text{PF}(s, S, T)$ ; and 2)  $\text{PF}(s, S, T \setminus \{t\}) \geq \text{PF}(s, S, T) - \text{PF}(t, S, T)$ .

*Proof.* With the definition of peeling flow, we have

$$\text{PF}(t, S, T) = \text{MFLOW}(S, T) - \text{MFLOW}(S, T \setminus \{t\}) \quad (9)$$

$$\text{PF}(s, S, T) = \text{MFLOW}(S, T) - \text{MFLOW}(S \setminus \{s\}, T) \quad (10)$$

Combining Equation 9 and Equation 10, we have the following.

$$\text{PF}(t, S, T) - \text{PF}(s, S, T) = \text{MFLOW}(S \setminus \{s\}, T) - \text{MFLOW}(S, T \setminus \{t\}) \quad (11)$$

Due to property 3, we have

$$\text{PF}(s, S, T \setminus \{t\}) = \text{MFLOW}(S, T \setminus \{t\}) - \text{MFLOW}(S \setminus \{s\}, T \setminus \{t\}) \geq 0 \quad (12)$$

Therefore,  $\text{MFLOW}(S, T \setminus \{t\}) \geq \text{MFLOW}(S \setminus \{s\}, T \setminus \{t\})$ . Moreover, with Equation 11, we have the following.

$$\begin{aligned}
 \text{PF}(t, S \setminus \{s\}, T) &= \text{MFLOW}(S \setminus \{s\}, T) - \text{MFLOW}(S \setminus \{s\}, T \setminus \{t\}) \\
 &\geq \text{MFLOW}(S \setminus \{s\}, T) - \text{MFLOW}(S, T \setminus \{t\}) \\
 &= \text{PF}(t, S, T) - \text{PF}(s, S, T)
 \end{aligned} \quad (13)$$

Similarly, we have  $\text{PF}(s, S, T \setminus \{t\}) \geq \text{PF}(s, S, T) - \text{PF}(t, S, T)$ .  $\square$

### C. Case Study: Densest Commute Flows in Grab-Posisi

**Dataset and graph construction.** To demonstrate that STDF is not restricted to financial transaction graphs, we conduct a case study on Grab-Posisi, a GPS trajectory dataset collected from Grab's ride-hailing operations in Southeast Asia [32]. We focus on the morning peak period (7–10 am) and discretize the city into coarse-grained urban zones corresponding to well-known residential and business areas. Each zone is represented as a vertex, and a directed edge  $(u, v)$  aggregates commute trips from origin zone  $u$  to destination zone  $v$ . The capacity  $C(u, v)$  equals the number of trips during the time window, and the timestamp  $\mathcal{T}(u, v)$  is derived from the departure times of the trips, yielding a temporal flow network.

**Query formulation.** Residential zones with high outbound commute volume (e.g., Jurong East, Clementi, Holland Village, Commonwealth, Redhill) are selected as the source set  $S$ , while major business districts with high inbound volume (e.g., Outram Park, City Center, Raffles) form the sink set  $T$ . We issue an STDF query  $(S, T, k)$  with a minimum group

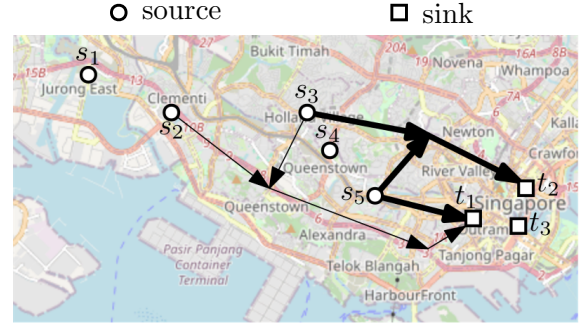


Fig. 19: Densest commute flow between residential and business zones on Grab-Posisi (morning peak) ( $s_1$ : Jurong East;  $s_2$ : Clementi;  $s_3$ : Holland Village;  $s_4$ : Commonwealth;  $s_5$ : Redhill;  $t_1$ : Outram Park;  $t_2$ : City Center;  $t_3$ : Raffles)

size constraint  $k$  to identify subsets  $S' \subseteq S$  and  $T' \subseteq T$  that maximize commute flow density under temporal feasibility.

**Findings.** Figure 19 visualizes the densest commute flow returned by STDF. Rather than selecting all high-volume zones, STDF identifies a compact subset of residential sources (e.g., Redhill and Holland Village) and business sinks (e.g., City Center and Outram Park) connected by a small number of dominant commute paths. These paths form a coherent west-to-central commute structure, reflecting the primary morning travel direction into Singapore's CBD. Compared with a volume-based baseline that ranks zones independently, the STDF result (i) concentrates substantially more flow per selected zone and (ii) yields a clearer, corridor-like spatial pattern instead of scattered origin–destination pairs. This case study illustrates that STDF captures structurally meaningful dense flows in urban mobility networks, demonstrating its applicability beyond financial transaction graphs.

### D. Network Reduction

**Definition A.1** (Temporal Flow). *In a TFN  $G = (V, E, C, \mathcal{T})$ , a temporal flow from a source  $s \in V$  to a sink  $t \in V$  is a pair of mapping functions  $\langle f, \mathcal{T} \rangle$  satisfying the following conditions:*

- 1) **Capacity Constraint:** Identical to Property (1) in Def. II.1.
- 2) **Flow Conservation:** At the final time  $\tau_{\max}$ , which marks the end of the period under consideration, the flow conservation property mirrors Property (2) in Def. II.1.
- 3) **Temporal Flow Constraint:**  $\forall u \in V \setminus \{s, t\}$  and  $\forall \tau \in [1, \tau_{\max}]$ , the cumulative flow entering  $u$  up to time  $\tau$  is at least as much as the flow leaving  $u$ :  

$$\sum_{e=(v,u) \in E, \mathcal{T}(e) \leq \tau} f(v, u) \geq \sum_{e=(u,v) \in E, \mathcal{T}(e) \leq \tau} f(u, v).$$

We propose a practical method to reduce the size of a TFN,  $G$ , to a smaller TFN,  $G'$ . We remark that the network reduction processing is done before evaluating the STDF queries.

**Edge Reduction.** We note that no temporal flow can occur through an outdated outgoing (resp. incoming) edge, as this would violate the temporal flow constraint (resp. flow conservation) when  $\tau = \mathcal{T}(u, v)$  (resp.  $\tau = \mathcal{T}(v, u)$ ). There are two kinds of outdated edges:  $\forall u \in V$ , a) its outgoing edge

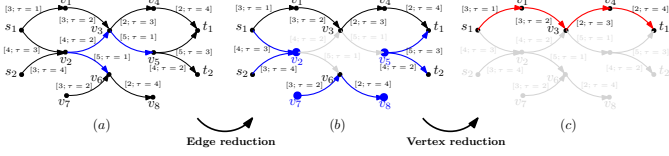


Fig. 20: A running example of network reduction

$e = (u, v)$  ( $u \notin S$  and  $v \notin T$ ) is outdated if  $\forall(v', u) \in E, \mathcal{T}(u, v) < \mathcal{T}(v', u)$ ; and b) its incoming edge  $e = (v, u)$  ( $v \notin S$  and  $u \notin T$ ) is outdated if  $\forall(u, v') \in E, \mathcal{T}(v, u) > \mathcal{T}(u, v')$ . All outdated edges are removed without affecting the answers to the STDF queries.

**Vertex Reduction.** A vertex  $u$  is a *flow inlet vertex* if its in-degree is 0 and  $u \notin S$ .  $u$  is a *flow outlet vertex* if its out-degree is 0 and  $u \notin T$ . Such vertices do not participate in any temporal flow and are hence removed.

**Reduction Process.** The network reduction process in a TFN,  $G$ , can be summarized by two key steps. The first step identifies all outdated edges and flow inlet and outlet vertices with a time complexity of  $O(|V|+|E|)$ . Then, the second step removes these outdated edges and vertices and, subsequently, any isolated vertices. This process effectively reduces the network's size, making subsequent analysis more efficient.

**Example A.1.** Consider a TFN with two sources,  $S = \{s_1, s_2\}$ , and two sinks,  $T = \{t_1, t_2\}$ , as depicted in Figure 20(a). To reduce the network, we first identify outdated edges by examining the timestamps of each edge. Noting that  $\mathcal{T}(v_2, v_6) = 1$  is less than both  $\mathcal{T}(s_1, v_2) = 3$  and  $\mathcal{T}(s_2, v_2) = 4$ , edge  $(v_2, v_6)$  is classified as outdated and is thus removed. Similarly, edges  $(v_2, v_3)$  and  $(v_3, v_5)$  are removed based on their timestamp comparisons as illustrated in Figure 20(b). In this process,  $v_5$  and  $v_7$  are identified as flow inlet vertices, and  $v_2$  and  $v_8$  as flow outlet vertices, leading to their removal. The reduced network is shown in Figure 20(c), on which the temporal flow  $\text{MFLOW}(S, T) = 2$  is efficiently computed.

### E. Network Compression

In this subsection, we propose a flow-preserving compression technique to reduce the size of the network. For ease of analysis, the vertices in RTFN are classified into three categories based on their in-degree and out-degree. We denote in-degree by  $\deg^{\text{in}}$  and out-degree by  $\deg^{\text{out}}$ .

- **Flow-out Vertices:**  $u$  is a flow-out vertex if 1)  $\deg^{\text{in}}(u) = 0$ , or 2)  $\deg^{\text{in}}(u) = 1$  and  $C(v, u) = +\infty$ , for  $(v, u) \in E$ .
- **Flow-in Vertices:**  $u$  is a flow-in vertex if 1)  $\deg^{\text{out}}(u) = 0$ , or 2)  $\deg^{\text{out}}(u) = 1$  and  $C(u, v) = +\infty$ , for  $(u, v) \in E$ .
- **Flow-crossing Vertices:**  $u$  is a flow-crossing vertex if  $\exists(u, v_1), (v_2, u) \in E, C(u, v_1) \neq +\infty$  and  $C(v_2, u) \neq +\infty$ .

**Vertex Compression (VCP( $G, u_1, u_2$ )).** Given an RTFN,  $G = (V, E, C)$ , the compression of two vertices  $u_1$  and  $u_2$  has the following steps:

- 1) Add a super vertex  $u$  to  $V$ .
- 2) If  $(v, u_1) \in E$  or  $(v, u_2) \in E$ , add  $(v, u)$  to  $E$ ; If  $(u_1, v) \in E$  or  $(u_2, v) \in E$ , add  $(u, v)$  to  $E$ .

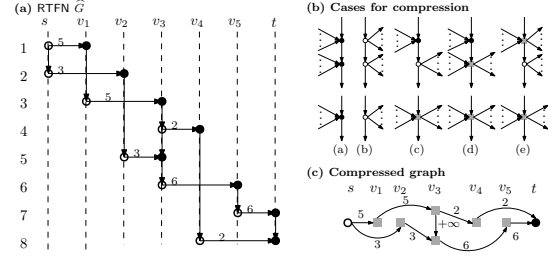


Fig. 21: The compressed graph of Figure 6(a)

- 3)  $u_1, u_2$ , and the edges adjacent to them are removed from  $E$ . The compression process is denoted by  $(G', u) = \text{VCP}(G, u_1, u_2)$ , where  $G'$  is the compressed graph and  $u$  is the super vertex.

Given a vertex compression  $(G', u) = \text{VCP}(G, u_1, u_2)$ , if  $u_1, u_2 \notin S \cup T$  and  $\text{MFLOW}(s, t)$  on  $G$  is equal to that on  $G'$  for any source  $s$  and sink  $t$ , then we say  $\text{VCP}(G, u_1, u_2)$  is *flow-preserving*.

**Network Compression (Algorithm 4, Figure 21).** We have discovered that there are five types of flow-preserving vertex compression. To illustrate these types in the compression, we color the flow-out vertices *white* and flow-in vertices *black* in Figure 21. The network compression of Conan scans each vertex  $u_1 \in V$  and checks if it can be compressed with any of its neighboring vertex  $u_2$ . If the compression of  $u_1$  and  $u_2$  fits any of the five flow-preserving cases, Conan compresses them using the function  $\text{VCP}(G, u_1, u_2)$ . The network compression process ends when no more vertices can be compressed. The time complexity of Algorithm 4 is  $O(|V|+|E|)$ .

**Lemma A.1.** Given a graph  $G$  and an edge  $(u_1, u_2) \in E$ , let  $(G', u) = \text{VCP}(G, u_1, u_2)$ . Then,  $(G', u)$  is flow-preserving in the following cases:

- **Case a.**  $u_1$  and  $u_2$  are both flow-in vertices; and  $u$  is a flow-in vertex.
- **Case b.**  $u_1$  and  $u_2$  are both flow-out vertices; and  $u$  is a flow-out vertex.
- **Case c.**  $u_1$  is a flow-in vertex; and  $u_2$  is a flow-out vertex.
- **Case d.**  $u_1$  is a flow-in vertex; and  $u_2$  is a flow-crossing vertex.
- **Case e.**  $u_1$  is a flow-crossing vertex; and  $u_2$  is a flow-out vertex.

**Proof Sketch.** The correctness of Lemma A.1 can be established by the following two lemmas:

- 1) If  $u_1$  is flow-in vertex or  $u_2$  is flow-out vertex,  $\text{VCP}(G, u_1, u_2)$  is flow-preserving. It is because either  $u_1$  has no other out-edge or  $u_2$  has no other in-edge,  $f(u_2, u_1) = 0$  regardless of  $C(u_2, u_1)$ , and thus,  $\text{VCP}(G, u_1, u_2)$  is flow-preserving.
- 2) If  $u_1$  and  $u_2$  are both flow-in (resp. flow-out) vertices, then for  $(G', u) = \text{VCP}(G, u_1, u_2)$ ,  $u$  is a flow-in (resp. flow-out) vertex. By the definition of vertex compression,  $u$  has at most one outgoing edge and its capacity is  $+\infty$ , which follows the definition of flow-in (resp. flow-out) vertices.

The detailed proof is shown in Appendix F of [2].

**Algorithm 4:** Network Compression

---

**Input:** An RTFN  $G = (V, E, C)$   
**Output:** A compressed network  $G'$

```

1 foreach  $u_1 \in V$  do
2   foreach  $u_2 \in N(u_1)$  do
3     if compression is flow-preserving for  $(u_1, u_2)$  then
4        $(G', u) = \text{VCP}(G, u_1, u_2)$ 
5       // Update color based on conditions
6       if  $u_1$  and  $u_2$  are both black then
7         color  $u$  black // Case a
8       else if  $u_1$  and  $u_2$  are both white then
9         color  $u$  white // Case b
10      else if  $u_1$  is black and  $u_2$  is white or  $u_1$  or  $u_2$  is gray
11        then
12          | color  $u$  gray // Cases c, d, e
11 return  $G'$ 
```

---

**Example A.2.** Consider the RTFN shown in Figure 6(a),  $s^1, s^2, v_1^3, v_2^5, v_3^4, v_4^6, v_5^8$  and  $v_5^7$  are flow-out vertices whereas  $v_1^1, v_2^2, v_3^3, v_4^4, v_5^5, v_6^3, v_7^7$  and  $t^8$  are flow-in vertices. We highlight the flow-out vertices white and flow-in vertices black as shown in Figure 21(a). Five flow-preserving vertex compression cases are presented in Figure 21(b). As the compression of  $s^1$  and  $s^2$  is an instance of **Case (b)**, they are compressed as illustrated in Figure 21(c). Similarly,  $(t^7, t^8)$  is an instance of **Case (a)** and  $(v_1^1, v_1^3)$  is an instance of **Case (c)**, they are compressed accordingly. The compressed graph is shown in Figure 21(c).

#### F. The proof of network processing

**Theorem IV.1.** Given a TFN  $G$  with a source  $s$  and a sink  $t$ , the maximum flow value  $\text{MFLOW}(s, t) = \text{MFLOW}(s^{\tau_1}, t^{\tau_{\max}})$  in the RTFN  $\hat{G}$ .

*Proof.* We prove this theorem by contradiction. Assume that the maximum flow from  $s^{\tau_1}$  to  $t^{\tau_{\max}}$  on RTFN is  $\hat{f}$  and the maximum flow from  $s$  to  $t$  on TFN is  $f$ . 1) If  $|\hat{f}| < |f|$ , there exists a flow  $\hat{f}'$  on RTFN, such that  $|\hat{f}'| = |f|$  by Lemma A.2.  $|\hat{f}'| > |\hat{f}|$  contradicts the assumption that  $\hat{f}$  is the maximum flow on RTFN. 2) If  $|\hat{f}| > |f|$ ,  $f$  is not the maximum flow on TFN using Lemma A.3 which contradicts the assumption. Hence, we conclude that  $|\hat{f}| = |f|$ .  $\square$

**Lemma A.2.** Given a TFN  $G$ , two vertex  $s$  and  $t$ , and any temporal flow  $f$  between  $s$  and  $t$ , there exists a flow  $\hat{f}$  with the same value between  $s^{\tau_1}$  and  $t^{\tau_{\max}}$  in RTFN  $\hat{G}$ , following the transformation function  $\text{TR}$ , where  $s^{\tau_1}$  is the first copy of  $s$  and  $t^{\tau_{\max}}$  is the last copy of  $t$ .

*Proof.* We prove this lemma using the construction method.

The transformation function (resp. the transformation reverse function) denoted as  $\text{TR}$  (resp.  $\text{TR}^{-1}$ ), is used to transform edges from TFN to RTFN (resp. from RTFN to TFN).

**Flow construction.** 1) Consider the edge  $e = (u, v)$  and  $\hat{E} = \text{TR}(e)$ . We let  $\hat{f}(\hat{E}) = f(e)$ . 2) Consider a vertex  $u \in V$  and its copies  $u^{\tau_1}, u^{\tau_2}, \dots, u^{\tau_k}$  in  $\hat{G}$ . We let  $\hat{f}(u^{\tau_i}, u^{\tau_{i+1}}) = \sum_{v \in V} \hat{f}(u, v) - \sum_{v \in V} \hat{f}(v, u)$ , where  $T(v, u) \leq \tau_i$  and  $T(u, v) \leq \tau_i$ . We show that the construction preserves capacity constraint and flow conservation.

**Capacity constraint.** Consider edge  $e = (u, v)$  and its transformed edge  $\hat{E} = \text{TR}(e)$ . **Case 1:**  $\hat{C}(\hat{E}) = C(e)$  implies

that  $\hat{f}(\hat{E}) = f(e) \leq C(e) = \hat{C}(\hat{E})$ . **Case 2:** Consider each vertical edge  $\hat{E} = (u^{\tau_i}, u^{\tau_{i+1}})$ . Since the temporal flow constraint in Definition A.1,  $\hat{f}(\hat{E}) \geq 0$ . Since the  $\hat{C}(\hat{E}) = +\infty$ ,  $0 \leq \hat{f}(\hat{E}) < \hat{C}(\hat{E})$ . Hence, the capacity constraint is preserved.

**Flow conservation.** Consider a vertex  $u \in V \setminus \{s, t\}$  and its copies  $u^{\tau_1}, u^{\tau_2}, \dots, u^{\tau_k}$  in  $\hat{G}$ . For a copy  $u^{\tau_{i+1}}$ , the incoming flows are either from 1)  $u^{\tau_i}$  or 2) the copies of other nodes. The outgoing flows are either to 1)  $u^{\tau_{i+2}}$  or 2) the copies to other nodes.

With the flow construction, the flow from  $u^{\tau_i}$  is

$$\hat{f}(u^{\tau_i}, u^{\tau_{i+1}}) = \sum_{v \in V, \tau \in (0, \tau_i]} f(v, u) - \sum_{v \in V, \tau \in (0, \tau_i]} f(u, v) \quad (14)$$

The flow from the copies of other nodes is

$$\hat{f}(v^{\tau_{i+1}}, u^{\tau_{i+1}}) = \sum_{v \in V, \tau = \tau_{i+1}} f(v, u) \quad (15)$$

The flow to  $u^{\tau_{i+2}}$  is

$$\hat{f}(u^{\tau_{i+1}}, u^{\tau_{i+2}}) = \sum_{v \in V, \tau \in (0, \tau_{i+1}]} f(v, u) - \sum_{v \in V, \tau \in (0, \tau_{i+1}]} f(u, v) \quad (16)$$

The flow to the copies of other nodes is

$$\hat{f}(u^{\tau_{i+1}}, v^{\tau_{i+1}}) = \sum_{v \in V, \tau = \tau_{i+1}} f(u, v) \quad (17)$$

By the Equation 14-17, we have

$$\hat{f}(u^{\tau_i}, u^{\tau_{i+1}}) + \hat{f}(v^{\tau_{i+1}}, u^{\tau_{i+1}}) = \hat{f}(u^{\tau_{i+1}}, u^{\tau_{i+2}}) + \hat{f}(u^{\tau_{i+1}}, v^{\tau_{i+1}}) \quad (18)$$

The sum of the incoming flow is equal to the outgoing flow. Hence, the flow conservation is preserved.  $\square$

**Lemma A.3.** Given a RTFN  $\hat{G}$ , two vertex  $s$  and  $t$ , and a flow  $\hat{f}$  between  $s$  and  $t$ . We can construct a flow  $f$  with the same value in the corresponding TFN.

*Proof.* We prove this lemma by construction method.

**Construction.** Consider edge  $\hat{E} = (u^{\tau_i}, v^{\tau_i}) \in \hat{E}$  and the original temporal edge  $e = \text{TR}^{-1}(\hat{E})$ . If  $\hat{f}(\hat{E}) \neq 0$ , we let  $f(e) = \hat{f}(\hat{E})$ . We show that the construction preserves capacity constraint, temporal flow constraint, and flow conservation.

**Capacity constraint.**  $\hat{C}(\hat{E}) = C(e)$  implies that  $f(e) = \hat{f}(\hat{E}) \leq \hat{C}(\hat{E}) = C(e)$ . Therefore, the capacity constraint is preserved.

**Temporal flow constraint.** Given a vertex  $u$ , we collapse all the copies  $u^{\tau_1}, u^{\tau_2}, \dots, u^{\tau_k}$ . Consider the timestamp  $\tau_i$ :

$$\hat{f}(u^{\tau_i}, u^{\tau_{i+1}}) = \sum_{v \in V, \tau \in (0, \tau_i]} f(v, u) - \sum_{v \in V, \tau \in (0, \tau_i]} f(u, v) \quad (19)$$

$\hat{f}(u^{\tau_i}, u^{\tau_{i+1}})$  is non-negative, we have

$$\sum_{v \in V, \tau \in (0, \tau_i]} f(v, u) \geq \sum_{v \in V, \tau \in (0, \tau_i]} f(u, v) \quad (20)$$

Therefore, the temporal flow constraint is preserved.

**Flow conservation.** The flow conservation is preserved that there is not outgoing from of  $u$  at timestamp  $\tau_k$ :

$$\sum_{v \in V, \tau \in (0, \tau_i]} f(v, u) = \sum_{v \in V, \tau \in (0, \tau_i]} f(u, v) \quad (21)$$

□

**Lemma A.4.** Given a TFN  $G = (V, E, C, \mathcal{T})$  and its RTFN  $\widehat{G} = (\widehat{V}, \widehat{E}, \widehat{C})$ , the size of  $\widehat{V}$  is bounded by  $2|E|$  and the size of  $\widehat{E}$  is bounded by  $3|E| - |V|$ .

*Proof.* Consider a vertex  $v \in V$ , there are  $\deg(v)$  copies in  $\widehat{G}$ . Hence, the number of the vertices in  $\widehat{G}$  is  $\sum_{v \in V} \deg(v) = 2|E|$ . The number of the vertical edges of a vertex  $v \in V$  is  $\deg(v) - 1$ , where  $\deg(v)$  is the degree of  $v$ . Hence, there are  $\sum_{v \in V} \deg(v) - 1 = 2|E| - |V|$ . And the number of horizontal edges is equal to  $|E|$ . Therefore, the number of  $\widehat{E}$  is  $3|E| - |V|$ . □

**Lemma A.5.** RTFN  $\widehat{G} = (\widehat{V}, \widehat{E}, \widehat{C})$ ,  $\widehat{G}$  is a DAG.

*Proof.* We prove this by contradiction. We assume there is a cycle in RTFN, denoted by  $(v_1, \dots, v_n)$ , where  $v_n = v_1$ . Based on the graph transformation, consider an edge  $e_i = (v_i, v_{i+1})$ . The y-axis (timestamp) of  $v_i$  is smaller than that of  $v_{i+1}$  if  $e$  is a vertical edge. The y-axis (timestamp) of  $v_i$  is equal to that of  $v_{i+1}$  if  $e$  is a horizontal edge. Therefore, the timestamp of  $v_1$  is smaller than or equal to that of  $v_n(v_1)$  by induction. Since there is at least one vertical edge, the timestamp of  $v_1$  is smaller than that of  $v_n(v_1)$ , which contradicts that the timestamp of each vertex is unique. Hence, RTFN is a DAG. □

**Lemma A.6.** Given a flow network  $G$  and an edge  $(u_1, u_2) \in E$ . If  $u_1$  is a flow-in vertex or  $u_2$  is a flow-out vertex,  $(G', u') = \text{VCP}(G, u_1, u_2)$  is flow-preserving.

*Proof.* Due to the definition of flow-in vertex and flow-out vertex, we have  $C(u, v) = +\infty$ . We denote the maximum-flow MFLOW( $s, t$ ) on  $G$  (resp.  $G'$ ) by  $f$  (resp.  $f'$ ). First, we prove that  $|f| \leq |f'|$ .

We assume that the minimum cut on  $G'$  is  $(S', T')$ , and let  $S = S' \setminus \{u'\}$ ,  $T = T' \setminus \{u'\}$ , we consider two cases.

- 1) If  $u' \in S'$ ,  $(S \cup \{u, v\}, T)$  is a cut with the same value on  $G$ .
- 2) If  $u' \in T'$ ,  $(S, T \cup \{u, v\})$  is a cut with the same value on  $G'$ .

Then, we prove that  $|f| \geq |f'|$ .

We assume that the minimum cut on  $G$  is  $(S, T)$ , and let  $S' = S \setminus \{u, v\}$ ,  $T' = T \setminus \{u, v\}$ , we consider 4 situations.

- 1) If  $u, v \in S$ ,  $(S' \cup u', T')$  is a cut with the same value on  $G'$ .
- 2) If  $u, v \in T$ ,  $(S', T' \cup u')$  is a cut with the same value on  $G'$ .
- 3) If  $u \in S, v \in T$ , the minimum cut contains the edge between  $u$  and  $v$ , the capacity of which is  $+\infty$ , therefore MFLOW( $G, s, t$ ) =  $+\infty$ , and thus MFLOW( $G, s, t$ )  $\geq$  MFLOW( $G', s, t$ ).
- 4) If  $u \in T, v \in S$ , because  $u$  only have one outgoing edge and it points to  $v$ , moving  $u$  from  $T$  to  $S$  will not increase the cut, therefore  $(S' \cup u', T')$  is a cut with the same value on  $G'$ . □

**Lemma A.7.** Given a flow network  $G$  and an edge  $(u_1, u_2) \in E$ . If  $u_1, u_2$  are flow-in vertices, then for  $(G', u') = \text{VCP}(G, u_1, u_2)$ ,  $u'$  is also an flow-in vertex.

*Proof.* All edges going out from  $u'$  is either from  $u$  or  $v$  from step 3 of combination. However, the only outgoing edge from  $u$  points to  $v$  is removed from step 1 (and if the outgoing edge of  $v$  points to  $u$ , it's also removed), therefore  $u'$  can either have no outgoing edge or have one outgoing edge with a capacity of  $+\infty$  which originally points from  $v$ , satisfying the condition of a flow-in vertex. □

**Lemma A.8.** Given a flow network  $G$  and an edge  $(u_1, u_2) \in E$ . If  $u_1, u_2$  are flow-out vertices, then for  $(G', u') = \text{VCP}(G, u_1, u_2)$ ,  $u'$  is also a flow-out vertex.

*Proof.* This lemma can also be proven by the reverse graph. In the reverse graph, all flow-in vertices change into flow-out vertices, and vice versa. We can prove that  $u'$  is a flow-in vertex on the reverse graph  $G'^T$  by lemma A.7, therefore  $u'$  on  $G'$  is a flow-out vertex. □

**Theorem A.9.** Given a TFN  $G^T = (V, E, C, T)$  and its RTFN after compression  $\widehat{G} = (\widehat{V}, \widehat{E}, \widehat{C})$ ,  $|\widehat{V}| \leq |E| + |V|$ ,  $|\widehat{E}| \leq 2|E|$ .

*Proof.* By construction of RTFN, for a vertex  $u \in V$ , its copies form a sequence  $\text{Seq} = \{u^{\tau_1}, u^{\tau_2}, \dots, u^{\tau_{\deg(u)}}\}$  and each vertex is painted either black and white. The size of the sequence can be reduced from  $k$  to  $\lfloor \frac{k}{2} \rfloor + 1$ .

We prove this by construction. First, combine all continuous vertices with the same color. Let  $\text{Seq}'$  denotes the sequence after this step, all adjacent vertices in  $\text{Seq}'$  then have different colors, and we have  $|\text{Seq}'| \leq |\text{Seq}|$ . Next, we combine all black vertices with their succeeding white vertices in  $\text{Seq}'$ . All vertices in  $\text{Seq}'$  except the possible leading white vertex and trailing black vertex combine with another vertex in this step. Let  $\text{Seq}''$  denote the sequence after this step. If  $|\text{Seq}'|$  is odd, there will be either a leading white vertex or a trailing black vertex, hence  $|\text{Seq}''| = \lfloor \frac{|\text{Seq}'|}{2} \rfloor + 1$ . If  $|\text{Seq}'|$  is even, there will be either no nodes cannot be combined or a leading white vertex and a trailing black vertex at the same time, hence  $|\text{Seq}''| = \lfloor \frac{|\text{Seq}'|}{2} \rfloor$  or  $|\text{Seq}''| = \lfloor \frac{|\text{Seq}'|}{2} \rfloor + 1$ . Therefore, we have  $|\text{Seq}''| \leq \lfloor \frac{|\text{Seq}'|}{2} \rfloor + 1 \leq \lfloor \frac{k}{2} \rfloor + 1$ .

With this proven, there will be  $\sum_{u \in V} \left( \lfloor \frac{\deg(u)}{2} \rfloor + 1 \right) \leq |E| + |V|$  vertices after compression. Also, for each pair of nodes combined, an edge with an infinite flow between the two combined nodes will also be removed, hence there will be at least  $|E| - |V|$  edges removed, and  $|\widehat{E}| \leq 2|E|$ . □

**Property 1.** Given two pairs of sources and sinks  $(s_1, t_1)$  and  $(s_2, t_2)$ , and the corresponding maximum flows  $f_1 = \text{MFLOW}(s_1, t_1)$  and  $f_2 = \text{MFLOW}(s_2, t_2)$ . If  $f_1$  and  $f_2$  are overlap-free, then  $f_1 + f_2 = \text{MFLOW}(\{s_1, s_2\}, \{t_1, t_2\})$ .

*Proof.* If  $f_1 + f_2 > \text{MFLOW}(\{s_1, s_2\}, \{t_1, t_2\})$ , we construct a flow  $f'$  that  $f'(u, v) = f_1(u, v) + f_2(u, v)$  with  $|f'| = |f_1| + |f_2| > \text{MFLOW}(\{s_1, s_2\}, \{t_1, t_2\})$ , and  $f'$  follows all conditions in II.1 because  $\text{REACH}(s_1, t_2) = \text{False}$  and  $\text{REACH}(s_2, t_1) = \text{False}$ . And if  $\text{MFLOW}(s_1, t_1) + \text{MFLOW}(s_2, t_2) < \text{MFLOW}(\{s_1, s_2\}, \{t_1, t_2\})$ , because  $\text{REACH}(s_1, t_2) = \text{False}$  and  $\text{REACH}(s_2, t_1) = \text{False}$ , flow goes out from  $s_1$  is equal to flow goes in to  $t_1$ , resp.  $s_2, t_2$ . Therefore either  $f_{out}(s_1) > \text{MFLOW}(s_1, t_1)$  or  $f_{out}(s_2) > \text{MFLOW}(s_2, t_2)$ . □